10-26-2010

Stability and Stabilization of Systems with Time Delay. Limitations and Opportunities

R. Sipahi

S.-I. Niculescu

C. T. Abdallah

W. Michiels

K. Gu

Stability and Stabilization of Systems with Time Delay

Limitations and opportunities

R. Sipahi, S.-I. Niculescu, C.T. Abdallah, W. Michiels, K. Gu

October 25, 2010

Control systems often operate in the presence of delays, primarily due to the time it takes to acquire the information needed for decision-making, to create control decisions, and to execute these decisions, as shown in Figure 1. Systems with delays arise in engineering, biology, physics, operations research, and economics.

In traffic-flow models, the drivers' delayed reactions, which combine sensing, perception, response, selection, and programming delays, must be considered [1–3]. These delays are critical in accounting for human behavior, analyzing traffic-flow stability, and designing collision-free traffic flow using adaptive cruise controllers [4].

Material distribution and supply-chain systems are composed of interconnected supply-demand points that share products and information in order to regulate inventories and respond to customer demands [5]. Sources of delay in supply chains include decision-making, transportation-line delivery, and manufacturing facilities that work with lead times [6]. These delays, which influence every stage of the supply-demand chain, deteriorate inventory regulation, thereby causing financial losses, inefficiencies, and reduced quality-of-service [7].

In process control, delay terms arise from mass-transport phenomena in stirred-tank reactors and flow-temperature-composition control [8, 9]. In milling processes, the flexibility of the cutting tool prevents a tooth from precisely machining the desired chip thickness, causing the following tooth to encounter the uncut portion of the chip in the form of an additional force [10, 11]. In this setting, the delay arises since the forces affecting the dynamics are associated with past events. In the milling process, the delay is the tooth-passing period, which is related to the spindle speed. If the

spindle speed is not correctly chosen, then undesirable vibrations, known as regenerative-chatter instability, occur at the interface of the metal workpiece and the cutting tool. This instability ultimately leads to increased tool wear, undesirable surface quality, and reduced productivity.

Delays arise in biology [12, 13] and population dynamics [14, 15]. For instance, a population can grow only after the offspring mature and become reproductive. Models of reaction chains and transport phenomena have delay terms since chemical reactions and mass transport occur after an interval of time. An example is the breathing process within the physiological circuit that controls the carbon-dioxide level in the blood [16,17]. Delay terms also model sensing times in human motor control [18, 19], HIV dynamics [20], circulation dynamics of hormones in the bloodstream [21], and the dynamics of chronic myelogenous leukemia [22]. This list of dynamical systems with delays is far from complete, and additional examples are presented and discussed throughout this article.

The presence of delays may be either beneficial or detrimental to the operation of a dynamical system. A feedback system that is stable without delay may become unstable for some delays [23, 24], yet, judicious introduction of a delay may stabilize an otherwise unstable system [11]. This paradox may explain the five decades of interest in the stability and control of delay systems [11, 25–33]. The potentially stabilizing effect of delays is a motivation for exploiting the ever-present delays in dynamical systems. For instance, appropriate adjustment of the spindle speed helps in tuning the delay to avoid chattering in metal machining, while intentionally adding delays to decision-making allows supply-chain managers to observe consumer trends in order to make better purchasing and stocking decisions [7]. This stability-seeking approach is known as the wait-and-act control strategy [34]. The presence of properly timed delays designed for waiting before executing a decision is an effective stabilizing control strategy. For example, prolonging delays in the feedback loop may help recover stability of an otherwise unstable system [35–38].

Interest in understanding the effects of delays and designing stabilizing controllers that account for delays is also increasing with the complexity of control systems [39–41]. In particular, the effect of delays becomes more pronounced in interconnected and distributed systems [42], where multiple sensors, actuators, and controllers introduce multiple deterministic and stochastic delays. In interconnected systems, delays may arise from the availability of shared communication networks, such as the Internet and wireless networks illustrated in Figure 2 [43]. Delays are also found in tele-operation [44], tele-surgery [45], the coordination of unmanned vehicles [46–50], decentral-

ized and collaborative control of multiple agents [51, 52], synchronization and haptics [53], adaptive combustion control [54], combustion dynamics in liquid-propellant motors [55], chemical processes with transport delays [56], active vibration suppression [57], and sway control in cranes [58].

The objectives and scope of this article are as follows. We discuss various problems and opportunities arising due to delays in linear time-invariant (LTI) systems modeled by delay differential equations (DDEs). We illustrate that intentional delays, when judiciously chosen, can be used to stabilize and improve the closed-loop response of these systems. We use eigenvalues, spectrum assignment, and parametric techniques to study stability. Lyapunov and linear matrix inequality techniques are considered in [59].

The remainder of this article is organized as follows. We first present models of linear time-invariant systems with multiple delays, and the resulting characteristic equations. We then illustrate the spectral properties of these systems using an example, and explain how this spectrum, and thus stability, is affected by a single delay and a single controller gain. Next, visualization of asymptotic stability in the form of stability charts is demonstrated. We then present two application examples. The first example concerns network systems, where delays arise from communication lines. The second example demonstrates a case of uncontrolled vibration in which delays are part of metal-machining dynamics. For each example, we illustrate how delays can have either a stabilizing or destabilizing effect. These examples serve as an introduction to more technical discussions regarding the limitations of designing controllers. Stability analysis in the presence of multiple delays is also discussed, including the robustness of Smith predictors with respect to uncertainty in the delays. Finally, we draw some conclusions and give a view of potential directions for future work. For notation used in the text, see "Notation".

1 Delay Differential Equations and the Characteristic Equation

Most models of systems with delays are obtained based on inflow-outflow interactions, such as conservation laws involving mass and energy. These models describe relationships among the rates of change of flow variables, as well as the balance among the corresponding inflow rates and outflow rates affected by delays. Inflow may be due to production and reproduction, while outflow may represent consumption, death, or elimination [11, 25, 28–30].

The examples we consider can be cast as the DDE

$$\frac{dx(t)}{dt} = A_0 x(t) + \sum_{i=1}^{N} A_i x(t - \tau_i), \tag{1}$$

where $x(t)$ is the n-dimensional state variable, A_i, $i = 0, \ldots, N$, is an $n \times n$ matrix with constant real entries, and N is a positive integer. In (1), $\tau_i > 0$ is the delay, that is, $\dot{x}(t)$ depends on $x(t)$ at time t as well as at the time instants $t - \tau_i$. The delay is a shift operator that lags an input signal by the constant amount of time τ_i as illustrated in Figure 3. This type of delay represents a first-in-first-out-type model found in sensing, information transmission, and mass transport.

1.1 Characteristic Equations

The characteristic equation of (1) is given by

$$f(s; \tau_1, \ldots, \tau_N) := \det \left[sI - A_0 - \sum_{i=1}^{N} A_i e^{-s\tau_i} \right] = 0, \tag{2}$$

where I is the $n \times n$ identity matrix, and the exponential functions arise from the Laplace transforms of the delay terms. Due to the presence of the exponential terms, (2) is a *quasi-polynomial*, and thus is a transcendental equation, which possesses an infinite number of roots in the complex plane $\mathbb{C}$, called *characteristic roots*.

For a given set of delays, (1) is asymptotically stable if and only if all of the roots of (2) lie in the open left-half complex plane $\mathbb{C}_-$. Verifying asymptotic stability can be difficult since (2) has infinitely many characteristic roots. To address this difficulty, continuity of the spectrum of (1) needs to be exploited [11, 25, 28, 40]. Henceforth, "stability" refers to asymptotic stability.

To illustrate how to analyze the stability of a DDE, consider the plant transfer function $H(s) = 1/s$ with the controller $C(s) = -ke^{-s\tau}$, where τ is the delay and k is the controller gain. The characteristic equation of this system is given by $f(s; \tau) := s + ke^{-s\tau}$. If $\tau = 0$, then $f(s; \tau) = 0$ has a single root at $s = -k$. As we increase τ from zero to 0^+, the root $s = -k$ moves in $\mathbb{C}$, while at the same time an infinite number of roots $s = \tilde{s}_i$, $i = 1, 2, \ldots$, appear in $\mathbb{C}$. These roots satisfy two conditions, namely, $\Re(\tilde{s}_i) < 0$, and $|\tilde{s}_i| \to \infty$, as $\tau \to 0^+$. That is, for an infinitesimally small delay, the roots $\tilde{s}_i$ are dormant from a stability point of view. As the delay

parameter increases, however, the real parts of these roots may increase, and consequently these roots can destabilize the closed-loop system.

To understand the movement of roots in $\mathbb{C}$, define $g : \mathbb{R}_+ \times \mathbb{R} \mapsto \mathbb{R}$ by

$$g(\tau; k) := \sup \left\{ \Re(s) : \quad f(s; \tau) := s + ke^{-s\tau} = 0, s \in \mathbb{C} \right\}. \tag{3}$$

The function $g(\tau; k)$, called the *spectral abscissa* function, defines the real part of the rightmost characteristic root, and the stability analysis reduces to checking the sign of $g(\tau; k)$. Furthermore, since $g(\tau; k)$ is a continuous function of both τ and k [26,31,60], it follows that the system can switch from stability to instability, or vice versa, only when at least one characteristic root moves to the imaginary axis as τ changes. That is, stability analysis of the system requires calculating the characteristic roots $s = \jmath\omega$ of the corresponding characteristic equation. This approach is the basis of the stability analysis of (1) using (2) [11, 39, 61, 62].

1.2 Stability Charts

When studying the stability of (1), one of the main objectives is to determine necessary and sufficient conditions for closed-loop stability in either the delay-parameter space or the controller-parameter space [63–65]. Characterization of stability in delay-parameter space relies on the τ-decomposition technique [66], while stability in controller-parameter space is studied using the D-decomposition principle [67]. These decomposition techniques state that boundaries in the parameter space exist to divide the space into regions, where all the values the parameter can attain in each region make the system either stable or unstable.

A DDE that is stable for only some values in the delay-parameter space is called *delay-dependent stable* [62]. If the stability of a DDE is maintained independently of the delay, then DDE is called *delay-independent stable*. Multiple disjoint delay regions may also exist, where the system may be stable within each region, while becoming unstable outside [68]. These regions, which are known as *stability regions*, become *stability intervals* in a system with a single delay, that is, when $N = 1$ in (1). Stability intervals can be detected using Kronecker summation [69], matrix pencils [33], frequency sweeping [40], and algebraic tools [68, 70].

Stability intervals can be extended to a 2D map, known as a stability chart [11], in which the intervals are displayed with respect to a controller gain, see Figure 4. A stability chart can also be obtained in the plane of two delays, where each delay arises from a different input-output system in the closed-loop control. Compared to the 1D stability analysis along

a single delay axis, the stability information in a 2D delay plane is richer since it represents whether a system is stable or not with respect to all combinations of delays. A stability chart can reveal whether increasing a delay value favors stability or instability. Moreover, for a fixed ratio τ_2/τ_1 between two delays, stability may be independent of the delays satisfying this ratio, although a small perturbation of this ratio may yield multiple switches from instability to stability. The sensitivity and existence of these special ratios is of practical interest when designing robust controllers.

Characterizing higher dimensional stability charts in delay-parameter space is challenging since the stability analysis of (1) is an NP-hard problem for $N > 1$ [71]. In this case, hardness is a computational measure of the amount of time or space it takes to solve an example of a decision question as a function of the size of its input. Nondeterministic polynomial (NP) hard problems are considered costly in this setting.

2 Examples of Systems with Delays

We now illustrate how delays appear either in engineered feedback systems, such as network control systems, or naturally as part of vibrational dynamics without the presence of feedback control. Further examples are discussed in "Delays in Microscopic Vehicular Traffic Flow", "Delays in Biology", and "Delays in Operations Research".

2.0.1 Networked Control Systems

Delays appear in parallel computation and computer networking. Distributed computing architectures use a network of computational elements to achieve performance levels that are not attainable by a single element. A distributed architecture is a cluster of computers communicating through a shared network [72]. In this context, the distribution of the computational load across available resources is referred to as *load balancing.*

Consider a computing network consisting of n computers, called nodes, which can communicate with each other. At startup, the nodes are assigned an equal number of tasks. Since some nodes may operate faster than others, load imbalance can occur. To balance the load, each node sends its queue size $q_j(t)$ to the remaining nodes in the network. Node i receives the information $q_j(t-\tau_{ij})$ from node j delayed by the length of time τ_{ij}. Node i then uses this information to compute its local estimate of the average number of tasks in the queues of the n nodes. This estimate, which is based on the observations, is given by $\frac{1}{n}\sum_{j=1}^{n} q_j(t-\tau_{ij})$ with $\tau_{ii}=0$. Node i then compares its queue

size $q_i(t)$ with its estimate of the network average in order to compute

$$\beta = q_i(t) - \frac{1}{n}\sum_{j=1}^{n} q_j(t - \tau_{ij}). \tag{4}$$

If β is greater than a nonnegative threshold β_i, then node i sends some of its tasks to the remaining nodes. If $\beta < \beta_i$, then no task is sent. Furthermore, the tasks sent by node i are received by node j with a task-transfer delay h_{ij}. The delay h_{ij}, which depends on the number of tasks to be transferred, is much greater than the communication delay τ_{ij}. The controller, that is, the load-balancing algorithm, decides how often and how fast to implement load balancing, and how many tasks are to be sent to each node.

In high-speed networks, load imbalance can also occur when multiple users attempt to compete for resources. For example, the congestion-dynamics model

$$\dot{X}(t) = Z(t - \tau_1) - \mu, \tag{5}$$

$$\dot{Z}(t) = -a(X(t - \tau_2) - \bar{X}) - b(X(t - \tau_2 - r) - \bar{X}), \tag{6}$$

represents a single connection between a communication source controlled by an access regulator and a distant node with a constant transmission capacity μ, where $X(t)$ denotes the buffer contents, $Z(t)$ is the current input rate, and $\bar{X}$ is the buffer target value. This model involves multiple delays, namely, τ_1, τ_2, and r, where the delay $\tau = \tau_1 + \tau_2$ is the round-trip time, and the delay r denotes the control-time interval, which can be manipulated in the network [73, 74].

2.0.2 Variable-Pitch Milling Dynamics

In the milling process shown schematically in Figure 5, the clamped metal workpiece is machined by a rotating cutting tool with several teeth. Since both the cutting tool and workpiece are deformable, each tooth leaves some uncut material, which then acts as an additional force on the following tooth. That is, a past event affects the evolution of the cutting dynamics. The delay in this context is defined by the tooth-passing period τ, which is proportional to the pitch angle between two consecutive teeth, and is inversely proportional to the rotational speed $\omega_{spindle}$ of the cutting tool.

A *regular-pitch cutting tool* with four flutes has four identical pitch angles at 90°, as shown in Figure 5(a). Under some cutting conditions and at some specific settings of $\omega_{spindle}$, regenerative-chatter instability occurs with the use of this cutting tool [10]. A tool with variable-pitch, which has unevenly

distributed pitch angles at 110°, 70°, 110°, 70° as shown in Figure 5(b), can remove this instability under the same conditions [10]. This design changes the tooth-passing periods between the teeth, that is, the delays. To extend the design, the pitch angles θ_1 and θ_2 can be considered as variables as shown in Figure 5(b), and the stability of the cutting dynamics can be investigated as a function of $\tau_1 = \theta_1/\omega_{spindle}$ and $\tau_2 = \theta_2/\omega_{spindle}$.

The characteristic equation of the variable-pitch milling dynamics with τ_1 and τ_2 is given by

$$f(s;\tau_1,\tau_2) = \det\left[I - \frac{1}{4\pi}\,K_t\,a(4 - 2(e^{-\tau_1 s} - e^{-\tau_2 s}))\Phi_0(s)\right] = 0, \qquad (7)$$

where K_t is a cutting-force coefficient, a is the axial depth-of-cut, the transfer matrix $\Phi_0(s)$ relates the forces on the tool to the displacement of the tool, and the exponential terms carry the effects of the tooth-passing periods τ_1 and τ_2 [75].

The model in (7) contains two independent delays, similar to the congestion-control dynamics. If the stability of the cutting dynamics is considered for a cutting tool with a fixed-pitch ratio n/m, then we can define a triplet (τ_0, m, n), such that $\tau_1 = m\tau_0$ and $\tau_2 = n\tau_0$. In this case, analysis of (7) reduces to a single-delay problem with respect to τ_0, resembling the stability analysis of the single integrator example presented in the section "Delay Differential Equations and the Characteristic Equation". It is, however, computationally overwhelming to solve (7) repeatedly for all pitch-ratios n/m. Determining the stability of multiple delay systems therefore requires different frameworks. Stability results for this variable-pitch milling example are given in the section "Multiple-Delay Case".

3 Destabilizing and Stabilizing Effects of Delays

We now explore the destabilizing and stabilizing effects of delays on the stability and control of DDEs. Single-delay systems with feedback laws are used to illustrate these concepts.

3.1 Destabilizing Effects of Delays

Consider the transfer function of a single integrator $H(s) = 1/s$ subject to the delayed controller $C(s) = -ke^{-\tau s}$ with $k > 0$. In order to determine the stability of the closed-loop system, we need to first find the roots $s = \jmath\omega$ of the closed-loop characteristic equation

$$s + ke^{-s\tau} = 0 \qquad (8)$$

for all τ, that is,

$$\cos(\omega\tau) = 0, \tag{9}$$

$$k\sin(\omega\tau) = \omega. \tag{10}$$

Due to the periodicity in (9)-(10), there exist infinitely many delays $\tau_{c,\ell} = \pi/(2k) + (2\pi\ell)/\omega_c$, $\ell = 0, 1, 2, \ldots$, all of which yield the crossing frequency $\omega_c = k$, that is, (8) has roots on the imaginary axis at $s = \pm\jmath k$. By continuity, it follows that closed-loop stability is guaranteed for all delays satisfying $\tau \in [0, \tau_c)$, where $\tau_c = \frac{\pi}{2k}$. In this example, the system is unstable for $\tau \geq \tau_c$, and thus τ_c is the *delay margin* of the system.

We now consider the movement of the rightmost root of (8) as τ changes. As shown in Figure 6 for the controller gain $k = 1$, increasing the delay from zero generates fast-moving characteristic roots, which enter from $-\infty$ in $\mathbb{C}$. Note that the root located at $-k$ for $\tau = 0$ moves to the left, as the delay increases. Finally, at the value $\tau_c = \pi/2$, a pair of roots entering from $-\infty$ crosses the imaginary axis toward $\mathbb{C}_+$. Larger values of k induce smaller delay margins, since $\tau_c = \pi/(2k)$. These results are confirmed by the Nyquist plot shown in Figure 7.

The number of unstable roots can be determined by studying the crossing direction of an imaginary root as a function of the delay parameter τ evaluated at the corresponding crossing frequency ω_c. Since the quantity $\Re\left\{\frac{ds}{d\tau}\right\}|_{s=\jmath\omega_c} = \omega_c^2$ is positive in this example, an increase of the delay beyond each critical delay value $\tau = \tau_{c,\ell}$ corresponds to the crossing of the imaginary axis by a pair of characteristic roots toward $\mathbb{C}_+$. The number NU of unstable roots can then be tracked as a function of delays. In this case, for a fixed value of k, NU increases by two each time the delay value increases past the critical delay value $\tau = \tau_{c,\ell}$. This analysis can be extended by considering different values of k and identifying the stability characteristics in the plane of τ versus k, as shown in Figure 8. The behavior of the characteristic roots can also be explained by using perturbation-based analysis [31, 76].

An alternative approach to handling more complicated multi-input, multi-output systems uses using matrix pencil techniques [31, 33, 40]. Yet another approach, which leads to the same conclusion, uses an algebraic transformation to reformulate the closed-loop characteristic polynomial as a one-parameter algebraic polynomial [68, 70]. This polynomial, which has the same imaginary roots as the original characteristic equation, can be analyzed using algebraic tools [16, 68, 77, 78].

3.2 Stabilizing Effects of Delays

Consider the second-order open-loop system $H(s) = 1/(s^2+\omega_0^2)$ in feedback with the delayed controller $C(s) = ke^{-\tau s}$ [79]. The closed-loop characteristic equation is given by

$$s^2 + \omega_0^2 - ke^{-s\tau} = 0. \tag{11}$$

If $\tau = 0$, then the system is unstable for all k. However, the system can be made stable either by designing appropriate values of k and τ [79], or by using a proportional-derivative controller without delay $C(s) = k_p + k_d s$.

We now design (k, τ) so that the closed-loop system is stable. As in (8), we can show that two distinct crossing frequencies exist for each $k > 0$, where $k \in (0, \omega_0^2)$, as given by $\omega_{c,1} = \sqrt{\omega_0^2 - k}$ and $\omega_{c,2} = \sqrt{\omega_0^2 + k}$, which lead to the critical delay values $\tau_{c,1,\ell} = (2\ell\pi)/\sqrt{\omega_0^2 - k}$ and $\tau_{c,2,\ell} = (2\ell + 1)\pi/\sqrt{\omega_0^2 + k}$, for $\ell = 0, 1, 2, \ldots$, respectively. The sensitivity expression $\Re\left\{\left[\frac{ds}{d\tau}\right]\right\}|_{s=\jmath\omega_c} = -\frac{2\omega_c^2}{\omega_0^2 - \omega_c^2}$ indicates that the characteristic roots crossing at $\omega_c = \omega_{c,1}$ favor stability, that is, the roots move toward $\mathbb{C}_-$, whereas the roots crossing at $\omega_{c,2}$ favor instability.

If $\tau = 0$, then the closed-loop system has only a pair of poles of the form $s = \pm\jmath\omega_{c,1}$. As calculated above, these poles favor stability at the delay values $\tau_{c,1,\ell}$. That is, for sufficiently small $\tau = \varepsilon > 0$, the closed-loop system becomes stable since the poles $s = \pm\jmath\omega_{c,1}$ move toward $\mathbb{C}_-$, and no closed-loop poles are located in $\mathbb{C}_+$ or on the imaginary axis. In this case, increasing the delay value has a stabilizing effect. Considering all critical delays, we conclude that the system is stable if and only if, for some nonnegative integer ℓ, the delay τ satisfies

$$\frac{2\ell\pi}{\sqrt{\omega_0^2 - k}} < \tau < \frac{(2\ell + 1)\pi}{\sqrt{\omega_0^2 + k}}.$$

We now study the behavior of the rightmost root of (11) as the delay value is increased from zero. To graphically demonstrate how stability is affected by the delay, we select $k = 1.5$ and $\omega_0 = 3$, and compute the real part of the rightmost root of the closed-loop system [80]. As shown in Figure 9, we see that the real part of the rightmost root changes its sign as the delay parameter varies, indicating the existence of multiple stability intervals along the delay axis. In this example, we have $\omega_{c,1} = \sqrt{7.5}$, and when the delay is perturbed from $\tau = 0$, the characteristic roots start moving from $s = \pm\jmath\sqrt{7.5}$ toward $\mathbb{C}_-$. For $0 < \tau < 0.9695$, these roots wander in $\mathbb{C}_-$, while, for $\tau = 0.9695$, the roots cross into $\mathbb{C}_+$, where they remain for $0.9695 < \tau < 2.2943$. These roots return $\mathbb{C}_-$ for several delay ranges as

shown in Figure 9. While this pair of roots exhibits this movement, the remaining characteristic roots do not cross the imaginary axis to $\mathbb{C}_+$, and consequently a finite number of stability intervals arise. When the parameter k is relaxed, we obtain the stability chart of the system shown in Figure 10. The stability intervals presented here can be calculated by methods surveyed in [81].

From a speed of response point-of-view, a comparison of the step responses in Figure 11 illustrates the possibility of a properly designed delayed proportional control $C(s) = ke^{-\tau s}$ matching the performance of the PD control $C(s) = k_p + k_d s$ as measured by the step response.

3.2.1 Delays as Derivative Feedback

Consider the linear system

$$\ddot{x}(t) - 0.1\dot{x}(t) + x(t) = u(t), \tag{12}$$

which is unstable for $u(t) = 0$ due to the negative damping term. The derivative feedback

$$u(t) = -k\dot{x}(t), \tag{13}$$

with $k > 0.1$ moves the unstable open-loop poles into the stable left-half plane. Alternatively, we can use the delayed-feedback control law

$$u(t) = x(t - r) - x(t), \tag{14}$$

which can be interpreted as a finite difference control law with a gain r, that is, $u(t) = -r\frac{x(t)-x(t-r)}{r}$. For small values of the delay r, (14) approximates the derivative control (13) with $k = r$. In fact, the system (12) is stabilized by moving the two right-half plane poles to the left-half plane for all $r \in (0.1002, 1.7178)$ [40]. This example demonstrates that by designing the controllers appropriately, closed-loop stability can be achieved by using delays to approximate the derivatives of signals [82].

A combination of m distinct delays can be used as a stabilizing strategy [37]. Consider the plant

$$x^{(n)}(t) = u(t), \tag{15}$$

which consists of a chain of integrators, and let the controller be chosen as

$$u(t) = -\sum_{i=1}^{m} k_i x(t - \tau_i). \tag{16}$$

For stabilizing (15), the delays can be arbitrarily large since we can scale the time variable as $t = \hat{t}/\rho$, where $\rho > 0$. That is, if (16) stabilizes (15), then we can find the controller

$$u(t) = -\sum_{i=1}^{n} \frac{k_i}{\rho} x(t - \rho\tau_i), \tag{17}$$

which also stabilizes (15). This result suggests an approach to designing the controller (17) for systems with arbitrarily large delays $\rho\tau_i$ [37]. We can first design (16) with appropriate gains k_i and sufficiently small delays τ_i. We can then calculate ρ, and compute the gains k_i/ρ of the controller (17).

An approximation of derivatives can be combined with a scaling of time [37], leading to the controller

$$u(t) = -\begin{pmatrix} \varepsilon^n q_0 & \frac{\varepsilon^{n-1} q_1}{(-1)} & \frac{2!\varepsilon^{n-2} q_2}{(-1)^2} & \cdots & \frac{(n-1)!\varepsilon q_{n-1}}{(-1)^{n-1}} \end{pmatrix} T^{-1}(\tau) \begin{pmatrix} x(t-\tau_1) \\ x(t-\tau_2) \\ \vdots \\ x(t-\tau_n) \end{pmatrix},$$

where $\varepsilon > 0$ is sufficiently small, τ_i, $i = 1, 2, ..., n$, satisfy $0 \leq \tau_1 < \tau_2 < \cdots < \tau_n$, q_i, $i = 0, 1, ..., n-1$, are chosen such that the closed-loop system with the derivative feedback control $u(t) = -\sum_{i=0}^{n-1} q_i x^{(i)}(t)$ is stable, and $T(\tau)$ is the Vandermonde matrix

$$T(\tau) = \begin{pmatrix} 1 & \tau_1 & \tau_2^2 & \cdots & \tau_1^{n-1} \\ 1 & \tau_2 & \tau_2^2 & \cdots & \tau_2^{n-1} \\ \vdots & \vdots & \vdots & \ddots & \vdots \\ 1 & \tau_n & \tau_n^2 & \cdots & \tau_n^{n-1} \end{pmatrix}.$$

While the controller (16) can stabilize (15), stabilization is not possible if $m < n$ [83].

Finally, consider the system $\dot{x}(t) = x(t) + u(t)$. The derivative feedback $u(t) = 2\dot{x}(t)$ stabilizes the system, but the closed-loop system is fragile to changes in the derivative feedback, where *fragility* is defined in the sense that stability is lost with the derivative approximation using finite differences, no matter how small the discretization step size is. Furthermore, it can be shown that no controller of the form $u(t) = H(x(t) - x(t - T))$, where the function $H(\cdot)$ is real, is able to stabilize the given system [84]. This conclusion demonstrates that, in some cases, using finite differences to approximate derivatives may not be valid [85].

3.2.2 Delays as Phase Synchronizers

The oscillator $\frac{1}{s^2+w^2}$ can be stabilized using the low-gain delayed feedback controller $C(s) = -\varepsilon e^{-s\tau}$, which provides the appropriate phase in the feedback loop. This approach is used to stabilize laser dynamics [86]. For multiple oscillators with the characteristic equation

$$\prod_{i=1}^{\nu}(s^2 + \omega_i^2) + \varepsilon e^{-s\tau} = 0, \tag{18}$$

where $\omega_i > 0,\ i = 1, \ldots, \nu$, the stabilization mechanism reduces to a phase-synchronization requirement using the delay parameter as explained next.

Consider the roots of the characteristic equation $H(s; \tau, \varepsilon) := f(s) + \varepsilon g(s) e^{-s\tau} = 0$ as a function of the gain $\varepsilon \in \mathbb{R}$ and the delay $\tau \geq 0$. Here, $f : \mathbb{C} \to \mathbb{C}$ and $g : \mathbb{C} \mapsto \mathbb{C}$ are entire functions. Then we have the following results [87].

Proposition 1 *Let $\hat{s}$ be a simple zero of f that is not a zero of g. Let $\mathcal{Q} \subset \mathbb{C}$ be a compact set that does not contain the zeros of f except $\hat{s}$, and such that the boundary of $\mathcal{Q}$ is a closed simple contour not containing $\hat{s}$. Then, for all $\hat{\tau} > 0$, there exists $\hat{\varepsilon} > 0$ such that $H(s; \tau, \varepsilon)$ has exactly one zero in $\mathcal{Q}$ for all $(\tau, \varepsilon) \in [0, \hat{\tau}] \times [-\hat{\varepsilon}, \hat{\varepsilon}]$. Furthermore, there exists a unique function $r : [0, \hat{\tau}] \times [-\hat{\varepsilon}, \hat{\varepsilon}] \to \mathcal{Q}$, $(\tau, \varepsilon) \mapsto r(\tau, \varepsilon)$ that satisfies $r(0, 0) = \hat{s}$ as well as $H(r(\tau, \varepsilon);\ \tau, \varepsilon) = 0$ for all $(\tau, \varepsilon) \in [0, \hat{\tau}] \times [-\hat{\varepsilon}, \hat{\varepsilon}]$. The function r can be decomposed as*

$$r(\tau, \varepsilon) = \hat{s} + \varepsilon\ \mu(\tau, \varepsilon), \tag{19}$$

where

$$\lim_{|\varepsilon| \to 0^+} \max_{\tau \in [0, \hat{\tau}]} \left| \mu(\tau, \varepsilon) + \frac{g(\hat{s})}{f'(\hat{s})} e^{-\hat{s}\tau} \right| = 0, \tag{20}$$

which denotes uniform convergence on compact delay intervals as $|\varepsilon| \to 0$.

Expressions (19)-(20) imply that, for small values of the gain parameter ε, the isolated zero $\hat{s}$ behaves as the function

$$\tau \mapsto \hat{s} - \varepsilon \frac{g(\hat{s})}{f'(\hat{s})} e^{-\hat{s}\tau}. \tag{21}$$

If the rightmost zeros of f are simple and lie on the imaginary axis, then the corresponding function (21) for each zero has a sinusoidal real part. As a consequence, stability for small values of ε depends on having an appropriate phase of these sinusoidal functions, which depends on only the delay parameter.

Proposition 2 *Assume that* $f(\bar{s}) = \overline{f(s)}$, $g(\bar{s}) = \overline{g(s)}$ *for all* $s \in \mathbb{C}$. *Let* $\gamma > 0$, *and assume that*

$$\lim_{R\to\infty} \sup \left\{ \left| \frac{g(s)}{f(s)} \right| : \ \Re(s) \geq -\gamma, \ |s| \geq R \right\} = 0. \tag{22}$$

Assume further that all zeros of f *are in the closed left-half plane. Denote by* $\jmath\omega_i$, $\imath = 1, \ldots, \nu$, *the zeros of* f *on the positive imaginary axis, each of which has multiplicity one. If the delay parameter* τ *is such that*

$$\Re \left(\frac{g(\jmath\,\omega_i)}{f'(\jmath\,\omega_i)} e^{-\jmath\,\omega_i \tau} \right) > 0, \tag{23}$$

for all $i = 1, \ldots, \nu$, *then all zeros of* $H(s; \tau, \varepsilon)$ *are in* $\mathbb{C}_-$ *for sufficiently small* $\varepsilon > 0$. *Finally, if the inequality in (23) is reversed, then the same claims hold for* $\varepsilon < 0$.

Example 1 *We consider the effects of time delays on the stability of a mechanical system [88]. The characteristic equation is given by*

$$H(s; \tau, \varepsilon) := f(s) + \varepsilon g(s) e^{-s\tau} := (s^2 + \omega_1^2)(s^2 + \omega_2^2) + \varepsilon s^2 e^{-s\tau} = 0. \tag{24}$$

For $\omega_1 = 2$ *and* $\omega_2 = 4$, *the functions* $\upsilon_i : \ \mathbb{R}_+ \to \mathbb{R}$ *given by*

$$\tau \mapsto \upsilon_i(\tau) = -\Re \left(\frac{g(\jmath\,\omega_i)}{f'(\jmath\,\omega_i)} e^{-\jmath\,\omega_i \tau} \right), \ i = 1, 2, \tag{25}$$

are depicted in Figure 12. Since $\deg(f(s)) > \deg(g(s))$, *assumption (22) of Proposition 2 is satisfied. According to Proposition 2, stability is achieved for sufficiently small positive values of* ε *when* $\upsilon_1(\tau) < 0$ *and* $\upsilon_2(\tau) < 0$, *that is, the delay* τ *satisfies*

$$\tau \in \bigcup \left\{ \left(\frac{\pi}{4} + k\pi, \ \frac{\pi}{2} + k\pi \right) : \ k \in \mathbb{N} \right\}. \tag{26}$$

Similarly, stability is achieved for sufficiently small negative values of ε *if either* $\upsilon_1(\tau) > 0$ *and* $\upsilon_2(\tau) > 0$, *or the delay* τ *satisfies*

$$\tau \in \bigcup \left\{ \left(\frac{\pi}{2} + k\pi, \ \frac{3\pi}{4} + k\pi \right) : \ k \in \mathbb{N} \right\}. \tag{27}$$

The intervals (26) and (27) are given in Figure 12. To illustrate the relation between the functions (25) and the behavior of the roots of (24) described by Proposition 1, we use the package DDE-BIFTOOL [80]. DDE-BIFTOOL

is a numerical stability and bifurcation analysis toolbox for DDEs that can compute the rightmost roots of their characteristic equations with respect to the delay parameter τ. We select two cases, namely, $\omega_1 = 2$ and $\omega_2 = 4$, where $\varepsilon = 1$ for both cases. This setting corresponds to [88, Example 5.1] with $\varepsilon = 1/4$. The plot of (25) with $\varepsilon = 1/4$ is provided in Figure 12, and the real part of the rightmost roots of (24) for $\varepsilon = 1$ is presented in Figure 13. Comparing these figures shows that the results are in agreement with the functions (25) depicted in Figure 12. Further details about DDE-BIFTOOL and similar packages are given in "Numerical Stability and Bifurcation Analysis". ■

We conclude this subsection by stating that proper tuning of the system parameters can lead to stability or improved behavior of a DDE. Beneficial effects of delays with different stabilizing mechanisms are found in designing predictors as explained in "Stabilizing Predictors", while the effects of delays on chaos prediction are discussed in "Stabilizing Unstable Periodic Orbits in Chaotic Systems".

4 Limitations in Control Design

4.1 Fundamental Limitations

Consider the stabilization of a strictly proper single-input single-output system described by the transfer function

$$H(s) := c(sI - A)^{-1}b = \frac{P(s)}{Q(s)}, \tag{28}$$

where (A, b, c) is a minimal state-space representation, Q is a polynomial of degree n, and P is a polynomial of degree $m < n$.

Let $C(s)$ be the transfer function of a possibly infinite-dimensional controller that stabilizes (28), and define the corresponding delay margin $D(P, C)$ by

$$D(P, C) := \sup\left\{\hat{\tau} \geq 0 : \ C \ \text{ stabilizes } H(s)e^{-s\tau} \text{ for all } \tau \in [0, \hat{\tau})\right\}.$$

The maximal allowable delay margin is defined as

$$DM(P) := \sup\left\{D(P, C) : \ C \text{ stabilizes } P\right\}.$$

The following result is based on [89, Theorems 7, 8, 14].

Theorem 1 *The maximal achievable delay margin of the plant (28) with a linear time-invariant controller is finite if and only if (28) has a pole in $\bar{\mathbb{C}}_+$ that is different from zero. Furthermore, if the plant has the unstable pole $s = re^{\jmath\phi}$ with $r > 0$ and $\phi \in \left[0,\ \frac{\pi}{2}\right)$, then*

$$DM(P) \leq \frac{\pi}{r}\sin\phi + \max\left(\frac{2}{r}\cos\phi, \frac{2}{r}\phi\sin\phi\right).$$

Example 2 *Consider the plant $H(s) = 1/(s+a)$ and the controller $C(s) = -ke^{-\tau s}$, where $a > 0$. The characteristic equation of the closed-loop system is given by $s + a + ke^{-s\tau} = 0$. By inspecting the stability of this system in (a, k), it follows that the system is stabilizable if and only if $a\tau < 1$ [31, Chapter 4]. According to Theorem 1, the maximal achievable delay margin over all stabilizing controllers is bounded by $2/a$. This result is obtained by explicitly constructing controllers that achieve a delay margin arbitrarily close to $2/a$ [89].* ■

Example 3 *For the multiple integrator $H(s) = 1/s^n$, the maximal achievable delay margin is infinite [90].* ■

4.2 Limitations of Controllers Based on Delayed Output Feedback

We now consider controllers based on the delayed output feedback

$$U(s) = -ke^{-s\tau}Y(s), \tag{29}$$

where $k \in \mathbb{R}$, $\tau \geq 0$, and the controller $C(s)$ is given by $C(s) = -ke^{-\tau s}$. We seek conditions on the pair (k, τ) such that the controller (29) stabilizes the system (28).

The following result is based on [83, Proposition III.3] and an extension of Lucas's theorem to classes of entire functions [91].

Proposition 3 *Let m be the degree of the polynomial $P(s)$ in (28). If (28) is stable with the control law (29), then the polynomial*

$$\gamma(s;\tau) := \sum_{k=0}^{m+1} \binom{m+1}{k} \frac{d^k Q(s)}{ds^k} \tau^{m+1-k}, \tag{30}$$

is Hurwitz.

Although the polynomial $\gamma(s;\tau)$ depends explicitly on the delay parameter τ, Proposition 3 provides conditions that do not depend on τ and k as demonstrated in the next example.

Example 4 *Consider the second-order system*

$$H(s) = \frac{1}{s^2 + a_1 s + a_2}. \tag{31}$$

In the notation of Proposition 3, $m = 0$ and $\gamma(s;\tau) = \tau s^2 + (a_1\tau + 2)s + (a_2\tau + a_1)$. The polynomial $\gamma(s;\tau)$ is Hurwitz if and only if $a_1\tau + 2 > 0$ and $a_2\tau + a_1 > 0$. These last two conditions are necessary for stabilizing (31) using (29) with k and τ as controller parameters. If these conditions are violated, that is, $a_1 \leq 0$ and $a_2 \leq a_1^2/2$, then (31) cannot be stabilized with the control law (29). ■

Corollary 1 *If the polynomial $Q(s)$ has at least one zero s_0 in $\bar{\mathbb{C}}_+$ with multiplicity at least $m+2$, then s_0 is a factor of $\gamma(s;\tau)$. In this case, $\gamma(s;\tau)$ is not Hurwitz stable and thus the plant (28) cannot be stabilized by the control law (29).*

Example 5 *The multiple integrator $H(s) = 1/s^n$ cannot be stabilized by the controller (29) for all $n \geq 2$, since in this case the degree m in P is equal to zero.*

If the control law includes n delays, that is, $U(s) = \sum_{i=1}^{n} k_i e^{-s\tau_i} Y(s)$, then the plant can be stabilized, as demonstrated in the subsection "Delays as Derivative Feedback". ■

4.2.1 Limitations of Controllers that Use Delays

For a given value of the gain k, we investigate whether or not the plant (28) with the control law (29) can be stabilized. In other words, we characterize the stability of the closed-loop system with the characteristic equation $Q(s) + ke^{-\tau s}P(s) = 0$, where the delay parameter τ is the only tunable parameter. We refer to this problem as the *delay stabilization problem*, and define two quantities that play a role in the solution of this problem, namely, $\text{card}(\mathcal{U}_+)$ and $\text{card}(\mathcal{S}_+)$, where $\text{card}(\mathcal{X})$ denotes the cardinality of $\mathcal{X}$. Here $\mathcal{U}_+$ is the set of the roots of $Q(s) + kP(s) = 0$ located in the closed right-half plane, and $\mathcal{S}_+$ is the set of strictly positive roots ω of the polynomial

$$F(\omega;k) = \mid Q(\jmath\omega) \mid^2 - k^2 \mid P(\jmath\omega) \mid^2 = 0. \tag{32}$$

For the delay stabilization problem, we invoke the following assumption [31, Chapter 11].

Assumption 1 *The gain $k \in \mathbb{R}$ satisfies the following conditions:*

1. *All roots of F are simple.*
2. *$0 \notin \mathcal{U}_+$.*
3. *$\mathrm{card}(\mathcal{U}_+) \neq 0$.*

Assumption 1 is used in Proposition 4 below. The derivation of Proposition 4 is based on sweeping the delay parameter from zero to infinity, combined with a continuity argument of the rightmost roots. The delay-stabilization problem is solvable if and only if there exists a delay $\hat{\tau} > 0$ such that the number of closed-loop characteristic roots in $\bar{\mathbb{C}}_+$ for $\tau = 0$, that is, $\mathrm{card}(\mathcal{U}_+)$, minus the net number of roots crossing the imaginary axis from $\mathbb{C}_+$ to $\mathbb{C}_-$ when the delay is varied over the interval $(0, \hat{\tau}]$ is equal to zero [31]. Note that $\mathrm{card}(\mathcal{S}_+)$ reflects imaginary-axis crossings of the roots. The crossing direction of these roots across the imaginary axis is independent of the delay values, that is, the crossing direction of each element of $\mathcal{S}_+$ is invariant. Furthermore, the crossing direction alternates over the ordered elements of $\mathcal{S}_+$ [62, Theorem 7].

For $\tau > 0$, define

$$n_+(\tau) = \sum_{\omega \in \mathcal{S}_+,\ F'(\omega) > 0} \mathrm{card}\left\{\mathcal{T}_\omega \cap (0, \tau]\right\}, \tag{33}$$

$$n_-(\tau) = \sum_{\omega \in \mathcal{S}_+,\ F'(\omega) < 0} \mathrm{card}\left\{\mathcal{T}_\omega \cap [0, \tau]\right\}, \tag{34}$$

where $\mathcal{T}_\omega$ is the set of delay values corresponding to each $\omega \in \mathcal{S}_+$. That is, the set $\mathcal{T} = \bigcup_{\omega \in \mathcal{S}_+} \mathcal{T}_\omega$ partitions the nonnegative delay space into intervals, where the number of roots in $\mathbb{C}_+$ is the same for each interval. Furthermore, let the sets $\mathcal{T}^+$ and $\mathcal{T}^-$ represent a partition of $\mathcal{T}$ as a function of the sign of the derivative F' evaluated at the corresponding crossing frequency, that is,

$$\mathcal{T}^+ = \bigcup_{\omega \in \mathcal{S}_+,\ F'(\omega) > 0} \mathcal{T}_\omega \setminus \{0\}, \quad \mathcal{T}^- = \bigcup_{\omega \in \mathcal{S}_+,\ F'(\omega) < 0} \mathcal{T}_\omega.$$

The following result characterizes stability with respect to the delay axis [31, Propositions 11.14, 11.18].

Proposition 4 *Let k satisfy Assumption 1. Then the delay-stabilization problem has a solution of the form (29) if and only if the following conditions hold:*

(i) $\mathrm{card}(\mathcal{U}_+(k))$ *is a positive even integer, which satisfies the inequality* $\mathrm{card}(\mathcal{U}_+(k)) \leq \mathrm{card}(\mathcal{S}_+(k))$.

(ii) At least one delay value $\hat{\tau} \in \mathcal{T}$ *exists, such that*

$$2n_-(\hat{\tau}) = 2n_+(\hat{\tau}) + \mathrm{card}(\mathcal{U}_+(k)). \tag{35}$$

In this case, for all delay values $\tau \in (\hat{\tau}, \hat{\tau}_+)$*, where*

$$\hat{\tau}_+ = \min\left(\mathcal{T}^+ \cap (\hat{\tau}, \infty)\right), \tag{36}$$

the closed-loop system is stable. Finally, if $\mathcal{S}_+ = \{\omega_+, \omega_-\}$*, where* $\omega_+ > \omega_-$*, then all stabilizing delay values are given by*

$$\tau \in (\underline{\tau_l},\ \overline{\tau_l}), \quad l = 0, 1, 2, \ldots, l_m, \tag{37}$$

where $\underline{\tau_l} = \tau_- + \frac{2\pi l}{\omega_-}$, $\quad \overline{\tau_l} = \tau_+ + \frac{2\pi l}{\omega_+}$*, and* $l_m = \left\lfloor \left\{ \frac{\omega_+\omega_-(\tau_+ - \tau_-)}{2\pi(\omega_+ - \omega_-)} \right\} \right\rfloor$.

Following Proposition 4, the limitations of using a delay as a controller parameter are displayed in Table 1.

5 The Multiple-Delay Case

In the case of multiple delays, the characteristic equation (2) becomes

$$f(s; \tau_1, \ldots, \tau_N) = \sum_{i=0}^{K} P_i(s)\, e^{-s \sum_{\ell=1}^{N} z_{k\ell}\, \tau_\ell} = 0\,, \tag{38}$$

where P_i are polynomials in s with real coefficients, $K \in \mathbb{Z}_+$, and $z_{i\ell} \in \mathbb{Z}_{0,+}$. Similar to the single delay case, in order to analyze stability transitions of the time-delayed dynamics, we study the imaginary roots $s = \jmath\omega$ of (38), where ω is nonnegative without loss of generality.

The set of frequencies ω such that $s = \jmath\omega$ is a root of (38) is the *crossing frequency set*, which is defined by

$$\overline{\Omega} = \{\omega \geq 0 \,|\, f(\jmath\omega; \tau_1, \ldots, \tau_N) = 0 \text{ for some } (\tau_1, \ldots, \tau_N) \in \mathbb{R}_+^N\}. \tag{39}$$

For each $\tilde{\omega} \in \overline{\Omega}$, there are infinitely many nonnegative delays of the form

$$(\tilde{\tau}_1, \tilde{\tau}_2, \ldots, \tilde{\tau}_N) + (p_1, p_2, \ldots, p_N)\, \frac{2\pi}{\tilde{\omega}}\,, \tag{40}$$

satisfying (38) with $s = \jmath\tilde{\omega}$, where $p_\ell \in \mathbb{Z}$, and $(\tilde{\tau}_1, \ldots, \tilde{\tau}_N)$ are the minimal positive delays. The periodicity $2\pi/\tilde{\omega}$ is due to the exponential terms in (38) at $s = \jmath\tilde{\omega}$. Considering all $\omega \in \overline{\Omega}$, the solutions in (40) lie on N-dimensional stability-switching hypersurfaces denoted by SSH.

As in the single-delay case, where the delay axis is decomposed into stability and instability intervals, in the multiple-delay case, the delay space is decomposed into stability and instability regions whose boundaries are determined by SSH. Nevertheless, SSH is not sufficient to determine the stability regions. A method for assessing the number of unstable roots of the system in the delay-parameter space is needed. Similar to the single-delay cases, sensitivity analysis on the SSH with respect to delays is needed, which is based on how imaginary roots $s = \pm\jmath\omega$ move across the imaginary axis. Keeping $\tau_1, \ldots, \tau_{\ell-1}, \tau_{\ell+1}, \ldots, \tau_N$ fixed, the sensitivity of $s = \pm\jmath\tilde{\omega}$ with respect to τ_ℓ is defined as

$$S(\tau_\ell) = \Re\left(\left.\frac{ds}{d\tau_\ell}\right|_{s=\jmath\tilde{\omega},\tilde{\tau}_1,\ldots,\tilde{\tau}_N}\right). \tag{41}$$

As the delay $\tau_\ell = \tilde{\tau}_\ell$ increases, the roots $s = \pm\jmath\tilde{\omega}$ move toward $\mathbb{C}_+$ if $S(\tau_\ell) > 0$, and toward $\mathbb{C}_-$ if $S(\tau_\ell) < 0$.

The sign of the sensitivity expression (41) is the same for all values of τ_ℓ in (40). That is, for a given $s = \pm\jmath\tilde{\omega}$ and $\tau_1, \ldots, \tau_{\ell-1}, \tau_{\ell+1}, \ldots, \tau_N$, the sensitivity expression (41) is invariant at infinitely many delay values $\tilde{\tau}_\ell + p_\ell\frac{2\pi}{\tilde{\omega}}$ [62, 78, 92].

5.1 The Two-Delay Case

We now present techniques that can be used to analyze the stability of DDEs with two delays. These are based on the discussions in the section "Delay Differential Equations and the Characteristic Equation".

5.1.1 Geometric Characterization

Consider the special case of (2) given by

$$f(s; \tau_1, \tau_2) = P_0(s) + P_1(s)e^{-\tau_1 s} + P_2(s)e^{-\tau_2 s} = 0, \tag{42}$$

where $P_i(s), i = 0, 1, 2$, are polynomials. In this example case, SSH become curves $\mathcal{C}$ in the τ_1-τ_2 plane. While a complete characterization of these curves is not always possible, the characteristics of $\mathcal{C}$ may be revealed in the case of (42) [92].

We rewrite (42) as

$$a(s;\tau_1,\tau_2) = 1 + a_1(s)e^{-\tau_1 s} + a_2(s)e^{-\tau_2 s} = 0, \tag{43}$$

where $a_i(s) = P_i(s)/P_0(s)$, $i = 1, 2$. For $s = \jmath\omega$, the three terms in (43) are vectors in the complex plane, the magnitudes of which are independent of τ_1 and τ_2. If (43) holds, then these vectors sum to zero, as shown in Figure 14. Furthermore, the last two terms in (43) can assume all possible orientations by adjusting the values of τ_1 and τ_2. Since the length of an edge of a triangle cannot exceed the sum of the two remaining edges, (43) is valid if and only if

$$|a_1(\jmath\omega)| + |a_2(\jmath\omega)| \geq 1 \tag{44}$$

and

$$-1 \leq |a_1(\jmath\omega)| - |a_2(\jmath\omega)| \leq 1. \tag{45}$$

The crossing frequency set $\overline{\Omega}$ can be identified as the set of ω that satisfy (44) and (45).

Example 6 *Consider the system*

$$a_1(s) = \frac{2.5}{s^2 + 2\zeta_1 s + 1}, \tag{46}$$

$$a_2(s) = \frac{1}{3s^2 + 6\zeta_2 s + 1}, \tag{47}$$

where $\zeta_1 = 1/\sqrt{2}$ *and* $\zeta_2 = 0.1$. *Figure 15 shows the plots of* $|a_1(\jmath\omega)| + |a_2(\jmath\omega)|$ *and* $|a_1(\jmath\omega)| - |a_2(\jmath\omega)|$ *with respect to* ω. *The crossing frequency set* $\overline{\Omega}$ *is identified from Figure 15 as* $\overline{\Omega} = \Omega_1 \cup \Omega_2$, *where* $\Omega_1 = [0.346, 0.758]$ *and* $\Omega_2 = [1.333, 1.650]$. ■

Note that $\mathcal{C}$ may consist of closed curves, spiral-like curves, and open-ended curves. In Example 6, the curves $\mathcal{C}_1$ corresponding to the set $\Omega_1 = [0.346, 0.758]$ give rise to closed-curves as shown in Figure 16. In the same example, the set Ω_2 leads to spiral-like curves $\mathcal{C}_2$, which may also run in different directions on the plane of delays, see Figure 17.

Example 7 *Consider the system*

$$a_1(s) = \frac{2}{s^2 + 2s + 1}, \tag{48}$$

$$a_2(s) = \frac{1.5}{16s^2 + 8s + 1}. \tag{49}$$

Figure 18 shows the plots of $|a_1(\jmath\omega)| + |a_2(\jmath\omega)|$ *and* $|a_1(\jmath\omega)| - |a_2(\jmath\omega)|$ *with respect to* ω*. In this case,* $\overline{\Omega}$ *contains two intervals, namely,* $\Omega_1 = (0, 0.197]$ *and* $\Omega_2 = [0.898, 1.079]$*, with the corresponding* $\mathcal{C}_1$ *in the form of open-ended curves as shown in Figure 19. Additional characteristics, such as smoothness of the curves* $\mathcal{C}$ *and the direction of imaginary-axis crossings of the characteristic roots, are discussed in [92].* ■

5.1.2 Stability of the Congestion-Control Dynamics

In the congestion control dynamics (5)-(6), the dynamics of the error variable $Y(t) = X(t) - \bar{X}$ are expressed by

$$\frac{d^2}{dt^2}Y(t) + aY(t-\tau) + bY(t-\tau-r) = 0. \tag{50}$$

We next investigate the stability of (50) in r-τ plane. The characteristic equation of (50) is given by

$$f(s;\tau,r) = s^2 + ae^{-\tau s} + be^{-(\tau+r)s} = 0. \tag{51}$$

Equation (51) is a special case of (42), where $P_0(s) = s^2$, $P_1(s) = a$, and $P_2(s) = b$ with $\tau_1 = \tau$ and $\tau_2 = \tau + r$. Using the geometric approach based on triangle inequalities illustrated above leads to the boundaries shown in r-τ plane in Figure 20. Sensitivity analysis reveals that the shaded parametric region determines where the congestion dynamics are stable. This example demonstrates how feedback with multiple delays can render an oscillatory open-loop system stable. The shape of the stability regions in the delay-parameter space (r, τ) is useful in choosing a *wait-and-act* strategy [74], which provides stability robustness with respect to the round-trip time τ.

5.1.3 An Approach Based on the Bilinear Transformation

In order to compute the characteristic roots on the imaginary axis, we replace the exponential terms in (38) with the bilinear transformation

$$e^{-\tau_\ell s} \to \frac{1 - T_\ell\, s}{1 + T_\ell\, s}. \tag{52}$$

The right-hand side of (52) is different from a first-order Padé approximation, which is restricted to $T_\ell = \tau_\ell/2$. In (52), we have $s = \jmath\omega$ and $T_\ell \in \mathbb{R}$, $\ell = 1, 2$. The transformation (52) is exact when the complex expressions on both sides of (52) agree in magnitude and phase [38,77,78,81]. Notice that,

if $s = \jmath\omega$, then the magnitudes agree for all τ_ℓ and T_ℓ. For the phases to agree, it is necessary that

$$(\tau_1, \tau_2) = \left(\frac{2\tan^{-1}(\omega T_1)}{\omega}, \frac{2\tan^{-1}(\omega T_2)}{\omega} \right) + (p_1, p_2)\,\frac{2\pi}{\omega}, \tag{53}$$

is satisfied, where $0 \leq \tan^{-1}(\cdot) < \pi$ and $\omega \in \overline{\Omega}$. In other words, the transformation (52) becomes exact for $s = \jmath\omega$, so long as (53) holds. Since the transformation (52) is exact, the imaginary roots of (38) can be studied using (52). Substituting (52) into (38) yields

$$g(s; T_1, T_2) = \sum_{m=0}^{M} Q_m(T_1, T_2)\, s^m = 0, \tag{54}$$

where $Q_m(T_1, T_2)$ are multinomials in terms of the parameters T_1 and T_2, and M is finite.

For $N = 2$ delays, we define the set

$$\Omega = \{\omega \geq 0 \,|\, g(\jmath\omega; T_1, T_2) = 0 \text{ for some } (T_1, T_2) \in \mathbb{R}^2\}, \tag{55}$$

which is analogous to (39).

Corollary 2 ([78]) *The set $\overline{\Omega}$ is identical to the set Ω.*

Corollary 2 indicates that finding $\overline{\Omega}$ from the transcendental equation (38) is equivalent to finding Ω from the algebraic equation (54). To find Ω, a Routh array is built using the coefficients $Q_1(T_1, T_2), \ldots, Q_M(T_1, T_2)$. The entries of this array are in terms of T_1 and T_2, and the roots $s = \jmath\omega$ of (54) can be expressed in terms of T_1 and T_2 by exploiting the rules of the array. Once all admissible (ω, T_1, T_2) solutions are identified numerically, obtaining (ω, τ_1, τ_2) is straightforward using (53).

Example 8 *Consider the characteristic equation*

$$f(s; \tau_1, \tau_2) = s^2 + s + 20 + (2\,s + 3)e^{-\tau_1 s} + (s + 4)e^{-\tau_2 s} + e^{-(\tau_1 + \tau_2)s} = 0, \tag{56}$$

in the parameter space of the delays (τ_1, τ_2). The equation corresponding to (54) is given by

$$\begin{aligned} g(s; T_1, T_2) = T_1\,T_2\,s^4 + (T_2 + T_1 - 2\,T_1\,T_2)s^3 + (1 + 14\,T_1\,T_2 + 2\,T_2)s^2 \\ + (18\,T_2 + 4 + 20\,T_1)s + 28 = 0, \end{aligned} \tag{57}$$

for which a Routh array is implemented to identify admissible (ω, T_1, T_2) *triplets. The points* (T_1, T_2) *are depicted in Figure 21(a). The third dimension in Figure 21(a) is the set* $\omega \in \overline{\Omega}$*, which is suppressed for clarity. With knowledge of* (ω, T_1, T_2)*, mapping back to the delay space is achieved using (53), as depicted in Figure 21(b). In Figure 21(b), the number NU of unstable roots is found with the help of (41).* ■

The periodicity $2\pi/\omega$ in (40) is the same as in (53), and suggests a classification of the curves in Figure 21(b). The minimum positive delay points mapped in this figure without $2\pi/\omega$ shifting are the generators of the remaining curves. These generators are called the *kernel curves*, while the remaining curves are called the *offspring*, which are identified by shifting the kernel curves on the τ_1-τ_2 plane with periodicity $2\pi/\omega$ for each $\omega \in \overline{\Omega}$. This classification is called *clustering* [78].

The presence of kernel and offspring curves formalizes the identification of stability transitions in multiple-delay systems. Stability transitions are captured with sole knowledge of the kernel curves and $\overline{\Omega}$. Stability transitions on the kernel curves map directly to the offspring curves. This mapping is due the invariance of the sensitivity expression in (41). With this simplification, the number of unstable roots in the plane of delays is identified.

To detect kernel and offspring curves, the Kronecker summation procedure [93, 94] and the building block procedure [77] can also be utilized. In the case of more than two delays, the kernel and offspring concepts remain the same, since these concepts are inherent to DDEs. In higher dimensional delay-parameter spaces, however, the kernel and offspring hypersurfaces become difficult to compute and characterize.

5.1.4 Stability of Variable-Pitch Milling Dynamics

Using the bilinear transformation, we determine the stability chart of the cutting dynamics with the characteristic equation (7) at one of the operating conditions. The stability chart is shown in Figure 22, where stable cutting options are in the shaded regions. In this figure, the positive slope of each line represents a pitch ratio of the cutting tool used in the machining process, and each line with a negative slope corresponds to a fixed speed of the cutting tool in revolutions per minute. Similar to Figure 21(b), the kernel and offspring curves are color coded in Figure 22. In this example, it suffices to capture the four disjoint kernel curves in order to generate all of the remaining curves in Figure 22. Each delay pair on the curves separating stability and instability renders the cutting dynamics a perfect oscillator at

the corresponding regenerative-chatter frequency ω_c, where $s = \jmath\omega_c$ is a root of (7). Modeling and stability analysis of regenerative-chatter dynamics are discussed in [10, 11, 95, 96].

5.2 Interference Phenomena

Interference among multiple delays affects stability. An example of constructive interference is when two delays do not destabilize a system even though each delay alone does [36]. This stability phenomenon with respect to one of the rays in the delay-parameter space is called the *delay interference* phenomenon [31,97,98]. Delay interference models capture the fragility, that is, the sensitivity, of the delay-independent stability property along a particular ray against arbitrary small perturbations of the direction of the ray [69,99].

To illustrate delay interference, consider the system

$$\dot{x}(t) = -x(t) - x(t-\tau_1) - \frac{1}{2}x(t-\tau_2). \tag{58}$$

The rays for which delay-independent stability property holds are represented by the axes $\tau_1 = 0$ and $\tau_2 = 0$ of the delay-parameter space, and by the particular ray $\tau_2 = 2\tau_1$. Consider first the case $\tau_2 = 0$ and $\tau_1 = \tau$, leading to the characteristic equation $s + 3/2 + e^{-s\tau} = 0$. Note that the delay-free system is stable since the characteristic root is located at $-5/2$. Moreover, the plot of $H(\jmath\omega) = -1/(\jmath\omega + 3/2)$ lies inside the unit circle, and therefore $|H(\jmath\omega)| \neq 1$ for all $\omega > 0$, and $1 - H(\jmath\omega)e^{-\jmath\omega\tau} \neq 0$ for all $\omega \in \mathbb{R}$ and all $\tau > 0$. In other words, the characteristic equation has no roots on the imaginary axis independent of the delay value τ, hence the corresponding DDE is delay-independent stable. A similar property holds when $\tau_1 = 0$ and $\tau_2 \neq 0$.

The analysis of (58) given in [33, 100] uses the Tsypkin frequency-sweeping criterion, which guarantees the robust stability of a closed-loop system with a stable single-input, single-output plant and a delayed unity feedback.

Consider next the case $\tau_2 = 2\tau_1 = 2\tau$. The corresponding characteristic equation becomes $s + 1 + e^{-s\tau} + 1/2e^{-2s\tau} = 0$. As in the previous case, we need to find the roots of $\jmath\omega + 1 + e^{-\jmath\omega\tau} + 1/2e^{-2\jmath\omega\tau} = 0$. In other words, we search for the solutions $z \in [-1, 1]$, $z = \cos(\omega\tau)$, to the equation $1/2z^2 + z + 1 = 0$ corresponding to the real part of the characteristic equation on the imaginary axis. It thus follows that $\jmath\omega + 1 + e^{-\jmath\omega\tau} + 1/2e^{-2\jmath\omega\tau} \neq 0$ for all $\omega \in \mathbb{R}$ and for all $\tau > 0$. In conclusion, the delay-independent stability arises for the ray $\tau_2 = 2\tau_1$ in the delay-parameter space.

Next, let the ray $\tau_2 = 2\tau_1$ be perturbed as $\tau_2 = (2+\varepsilon)\tau_1$ for $\varepsilon > 0$. We know that (58) is not stable for all positive delays τ_1 and τ_2. For instance, $s = \jmath/2$ is an eigenvalue of (58) when $\tau_1 = 2\pi$ and $\tau_2 = 3\pi$. The question then becomes whether the ray $\tau_2 = (2+\varepsilon)\tau_1$ is stable or not, or whether or not this ray intersects some boundaries separating stable and unstable regions. To answer this question, the limit of a sequence $\{\varepsilon_n\}_{n\geq 1} \to 0$ can be shown to exist, where $\varepsilon_n = 1/(2(2n+1))$, such that the ray with $\varepsilon = \varepsilon_n$ causes instability [31]. More precisely, for some delay values $\tau_1 > 2(2n+1)\pi$, the system becomes unstable on the ray corresponding to $\varepsilon = \varepsilon_n$. This instability is confirmed with the solution $s = \jmath/2$ with $\tau_1 = 2(2n+1)\pi$ [99].

Consider now the system

$$\dot{x}(t) = -ax(t) - x(t-\tau_1) - \frac{1}{2}x(t-\tau_2), \tag{59}$$

which recovers (58) when $a = 1$. Here we consider a as a positive parameter, and find that the delay-independent stability of (59) is confirmed for all $a \geq 3/2$ [31]. In particular, for all $a \geq 3/2$, $\mid H_1(\jmath\omega) \mid + \mid H_2(\jmath\omega) \mid < 1$ for all $\omega > 0$, where $H_1 = 1/(a+\jmath\omega)$ and $H_2(\jmath\omega) = 1/2(a+\jmath\omega)$. Therefore, $1+H_1(\jmath\omega)e^{-\jmath\omega\tau_1}+H_2(\jmath\omega)e^{-\jmath\omega\tau_2} \neq 0$ for all $\omega \in \mathbb{R}$, $\tau_1 > 0$, and $\tau_2 > 0$. Since the delay-free system is stable, the last assertion allows concluding delay-independent stability for all $\tau_1 > 0$ and all $\tau_2 > 0$ by extending Tsypkin's criterion to the multiple-delay case [40, 60, 100, 101].

For $a = 1$, only three stable rays exist. These rays are the axis $O\tau_1$ with $\tau_2 = 0$, the axis $O\tau_2$ with $\tau_1 = 0$, and the ray $\tau_2 = 2\tau_1$. In Figure 23, stability and instability regions of (59) in the delay-parameter space are presented for both $a = 1$ and $a = 1.3$. The solid lines, which are SSHs, correspond to delay values for which characteristic roots are on the imaginary axis. The dashed lines indicate the stable rays. Notice that small perturbations in the slope of stable rays lead to intersections with SSH, which is a consequence of the delay-interference phenomenon. As $a \to 3/2$, the number of stable rays increases and becomes arbitrarily large. For $a = 3/2$, the system becomes delay-independent stable [98].

5.2.1 Interference Mechanism in the Smith Predictor

In light of the results presented above, we consider the standard Smith predictor [32, 102, 103] for the transfer function $H(s) = H_0(s)e^{-s\tau}$, where $H_0(s)$ is a strictly proper stable transfer function and the delay τ is not exactly known. Assume that the delay-modeling error is bounded by some $\delta > 0$, that is, $|\tau - \tau_n| \leq \delta$, where τ_n is the nominal-delay value, and let $C_0(s)$

be a stabilizing controller for $H_0(s)$. The Smith controller computed for the nominal delay case $\tau = \tau_n$, by assuming that the system $H_0(s)$ contains no modeling errors and uncertainties, has the form

$$C(s) = \frac{C_0(s)}{C_0(s)H_0(s)(1 - e^{-s\tau_n})}.$$

Let $H_{cl,0}(s) = C_0(s)H_0(s)/(1 + C_0(s)H_0(s))$ be the transfer function of the delay-free closed-loop system. For the uncertain delay case, the transfer function of the closed-loop system is

$$H_{cl}(s) = \frac{H_{cl,0}(s)e^{-s\tau}}{1 - H_{cl,0}e^{-s\tau_n}(1 - e^{-s(\tau-\tau_n)})}.$$

The stability of $H_{cl}(s)$ is determined from the zero locations of the meromorphic function $1 - H_{cl,0}(s)e^{-s\tau_1} + H_{cl,0}(s)e^{-\tau_2}$, where $\tau_2 = \tau$ and $\tau_1 = \tau_n$. Note that, if the closed-loop system is not practically stable, that is, if there exists a frequency $\omega_0 > 0$ such that $|H_{cl,0}(\jmath\omega_0)| > 1/2$, then the ray $\tau_2 = \tau_1$ is subject to interference phenomena [104]. Extensions of the Smith predictor are given in [105].

5.3 Extension to Large Number of Delays

Stability studies of three-delay and four-delay DDEs are given in [56, 93, 94, 106–108]. Furthermore, the stability of a special case of (38) of the form

$$f(s; \tau_1, \ldots, \tau_N) = P_0(s) + \sum_{i=1}^{N} P_i(s)e^{-s\tau_i} = 0, \tag{60}$$

where N is arbitrarily large, can be analyzed using geometric methods [109]. If $N = 3$, then one way to analyze stability is to follow the ideas of the geometric characterization discussed above using triangle inequalities for two-delay cases [107]. The 3D geometries of the SSH that arise from this characterization are in the form of pipes with holes, connectors, caps, and semi-open pipes. Direct extensions of the existing methods to analyzing stability of systems with a large number of delays is not straightforward [33, 109], and existing results remain inconclusive in addressing stability in multiple-delay-parameter space.

6 Concluding Remarks

In this article, we analyzed the effects of delays in various dynamical systems modeled by linear time-invariant delay differential equations. The presenta-

tion focused on eigenvalue locations and parametric techniques rather than Lyapunov-based approaches. Examples from biology, networks, manufacturing systems, supply chains, and vehicular traffic flow are used to illustrate the limitations and potential advantages of delays. The beneficial effects of delays are explained by interpreting delays as phase synchronizers and as approximate derivatives. While we limit the article to the effects of delays on stability, results on improving tracking performance using delays also exist [110]. Delays are also discussed in the context of designing predictors as well as controllers for nonlinear systems. We feel that this area deserves further research. As an example, an approach to obtaining predictive dynamical systems models using time-delay embedding is provided [111]. The impact of delays continue to grow in many fields, including the control of distributed systems such as energy and computing grids [112–114].

References

[1] A. Bose and P. A. Ioannou, "Analysis of Traffic Flow with Mixed Manual and Semi Automated Vehicles," *IEEE Transactions on Intelligent Transportation Systems,* 4(4), pp. 173-188, 2003.

[2] M. Green, "How Long Does It Take to Stop?" *Transportation Human Factors*, vol. 2, pp. 231-253, 2000.

[3] M. Bando, K. Hasebe, A. Nakayama, A. Shibata, and Y. Sugiyama, "Dynamical Model of Traffic Congestion and Numerical Simulation," *Physical Review E,* vol. 51, pp. 1035-1042, 1995.

[4] M. Treiber, A. Kesting, and D. Helbing, "Delays, Inaccuracies and Anticipation in Microscopic Traffic Models", *Physica A,* vol. 360, no. 1, 71-88, 2006.

[5] J. Bélair and M. C. Mackey, "Consummer Memory and Price Fluctuations in Commodity Markets: An Integrodifferential Model," *J. Dynamics Diff. Eqs.,* vol. 1, pp. 299-325, 1989.

[6] C. E. Riddalls and S. Bennett, "The Stability of Supply Chains," *International Journal of Production Research*, vol. 40, pp. 459-475, 2002.

[7] J. D. Sterman, *Business Dynamics: Systems Thinking and Modeling for a Complex World*, McGraw-Hill, Boston, 2000.

[8] E. F. Camacho and C. Bordons, *Model Predictive Control in the Process Industry*, Springer-Verlag, London, 1995.

[9] D. M. Prett and M. Morari, *Shell Process Control Workshop*, Butterworths, 1987.

[10] Y. Altintas, S. Engin, and E. Budak, "Analytical Stability Prediction and Design of Variable Pitch Cutters," *ASME Journal of Manufacturing Science and Engineering,* vol. 121, pp. 173-178, 1999.

[11] G. Stépán, *Retarded Dynamical Systems: Stability and Characteristic Function.* Longman Scientific, UK, 1989.

[12] E. D. Sontag, "Some New Directions in Control Theory Inspired by Systems Biology," *Systems Biology,* vol. 1, pp. 9-18, 2004.

[13] C. T. H. Baker, G.A. Bocharov, and F.A. Rihan, *A Report on the Use of Delay Differential Equations in Numerical Modelling in the Biosciences.* Numerical Analysis Report No. 343, Manchester Centre for Computational Mathematics, Manchester, UK (1999). Available at `http://citeseer.ist.psu.edu/old/523220.html`

[14] Y. Kuang, *Delay Differential Equations with Applications in Population Dynamics.* Academic Press, Boston, 1993.

[15] K. Gopalsamy, *Stability and Oscillations in Delay Differential Equations of Population Dynamics.* Kluwer Academic Publishers, 1992.

[16] N. MacDonald, *Biological Delay Systems: Linear Stability Theory.* Cambridge University Press, Cambridge, 1989.

[17] B. Vielle and G. Chauvet, "Delay Equation Analysis of Human Respiratory Stability," *Math. Biosciences,* vol. 152, 105-122, 1998.

[18] T. D. Frank, R. Friedrich, and P. J. Beek, "Identifying and Comparing States of Time-Delayed Systems: Phase Diagrams and Applications to Human Motor Control Systems," *Physics Letters A,* vol. 338, pp. 74-80, 2005.

[19] K. Masani, A. H. Vette, N. Kawashima, and M. R. Popovic, "Neuromusculoskeletal Torque-Generation Process Has a Large Destabilizing Effect on the Control Mechanism of Quiet Standing," *Journal of Neurophysiology,* vol. 100, pp. 1465-1475, 2008.

[20] S. Yi, P. W. Nelson, and A. G. Ulsoy, "Eigenvalues and Sensitivity Analysis for a Model Of Hiv-1 Pathogenesis with an Intracellular Delay," in *Proceedings of the ASME Dynamic Systems and Control Conference,* Ann Arbor, MI, 2008, pp. 573-581.

[21] R. V. Culshaw, S. Ruan, and G. Webb, "A Mathematical Model of Cell-to-Cell Spread of HIV-1 that Includes a Time Delay," *Journal of Mathematical Biology,* vol. 46, pp. 425-444, 2003.

[22] D. Levy, S.-I. Niculescu, P. Kim, and K. Gu, "On the Stability Crossing Boundaries of Some Delay Systems Modeling Immune Dynamics in Leukemia", *Proc 17th International Symposium on Mathematical Theory of Networks and Systems,* Kyoto, Japan, 2006, pp. 2637-2647.

[23] H. Logemann and S. Townley, "The Effect of Small Delays in the Feedback Loop on the Stability of Neutral Systems," *Systems & Control Letters,* vol. 27, pp. 267-274, 1996.

[24] W. Michiels, K. Engelborghs, D. Roose, and D. Dochain, "Sensitivity to Infinitesimal Delays in Neutral Equations," *SIAM Journal on Control and Optimization,* vol. 40, pp. 1134-1158, 2002.

[25] R. E. Bellman and K. L. Cooke, *Differential-Difference Equations.* Academic Press, New York, 1963.

[26] R. Datko, "A Procedure for Determination of the Exponential Stability of Certain Differential-Difference Equations," *Quarterly Applied Mathematics,* vol. 36, pp. 279-292, 1978.

[27] A. Halanay, *Differential Equations; Stability, Oscillations, Time Lags*, Academic Press, New York, 1966.

[28] J. K. Hale and S. M. Verduyn Lunel, *Introduction to Functional Differential Equations.* Springer-Verlag, New York, 1993.

[29] N. N. Krasovskii, *Stability of Motion.* Stanford University Press, 1963.

[30] O. Diekmann, S. A. van Gils, S. M. Verduyn-Lunel, and H.-O. Walther, *Delay Equations, Functional-, Complex and Nonlinear Analysis.* Springer-Verlag, New York, 1995.

[31] W. Michiels and S.-I. Niculescu, *Stability and Stabilization of Time-Delay Systems. An eigenvalue approach.* SIAM, Philadelphia, 2007.

[32] O. J. M. Smith, "Closer Control of Loops with Dead Time," *Chemical Engineering Progress*, vol. 53, pp. 217-219, 1957.

[33] S.-I. Niculescu, *Delay Effects on Stability: A Robust Control Approach.* Springer-Verlag, Heidelberg, 2001.

[34] G. Stepan and T. Insperger, "Stability of Time-Periodic and Delayed Systems - A Route to Act-and-Wait Control", *Annual Reviews in Control,* vol. 30, pp. 159-168, 2006.

[35] J. Beddington and R. M. May, "Time Lags are not Necessarily Destabilizing," *Mathematical Biosciences,* vol. 27, pp. 109-117, 1975.

[36] N. MacDonald, "Two Delays may not Destabilize although either Delay can," *Mathematical Biosciences*, vol. 82, pp. 127-140, 1986.

[37] S.-I. Niculescu and W. Michiels, "Stabilizing a Chain of Integrators Using Multiple Delays," *IEEE Transactions on Automatic Control*, vol. 49, pp. 802-807, 2004.

[38] N. Olgac, R. Sipahi, and A. F. Ergenc, "'Delay Scheduling', an Unconventional Use of Time Delay for Trajectory Tracking", *Mechatronics,* vol. 17, pp. 199-206, 2007.

[39] T. Erneux, *Applied Delay Differential Equations.* Springer-Verlag, New York, 2009.

[40] K. Gu, V. L. Kharitonov, and J. Chen, *Stability of Time-Delay Systems.* Birkhauser, Boston, 2003.

[41] J. J. Loiseau, S.-I. Niculescu, W. Michiels, and R. Sipahi, (Eds.) *Topics in Time Delay Systems, Analysis, Algorithms and Control.* Springer-Verlag, Heidelberg, 2009.

[42] R. M. Murray, *Control in an Information Rich World: Report of the Panel on Future Directions in Control, Dynamics, and Systems.* SIAM, Philadelphia, PA, 2003.

[43] F. P. Kelly, "Mathematical Modelling of the Internet," pp. 685-702 in *Mathematics Unlimited - 2001 and Beyond.* B. Engquist, W. Schmid (Eds.), Springer-Verlag, Berlin, 2001.

[44] R. J. Anderson and M. W. Spong, "Bilateral Control of Teleoperators with Time Delay," *IEEE Transactions on Automatic Control,* vol. 34, pp 494-501, 1989.

[45] J. E. Speich and J. Rosen, *Medical Robotics.* Marcel Dekker, Inc., NY, 2004.

[46] R. M. Murray, "Recent Research in Cooperative Control of Multivehicle Systems", *ASME Journal of Dynamic Systems, Measurement and Control,* vol. 129, pp. 571-583, 2007.

[47] A. Papachristodoulou and A. Jadbabaie, "Synchronization in Oscillator Networks with Heterogeneous Delays, Switching Topologies and Nonlinear Dynamics," in *Proceedings of the IEEE Conference on Decision and Control,* San Diego, 2006, pp. 4307-4312.

[48] A. Jadbabaie, J. Lin, and A. S. Morse, "Coordination of Groups of Mobile Autonomous Agents Using Nearest Neighbor Rules," *IEEE Transactions on Automatic Control,* vol. 48, pp. 988-1001, 2003.

[49] R. Olfati-Saber and R. M. Murray, "Consensus Problems in Networks of Agents with Switching Topology and Time-Delays, *IEEE Transactions on Automatic Control,* vol. 49, pp. 1520-1533, 2004.

[50] U. Munz, A. Papachristodoulou, and F. Allgower, "Consensus Reaching in Multi-Agent Packet-Switched Networks with Nonlinear Coupling," *International Journal of Control*, vol. 82, pp. 953-969, 2009.

[51] W. B. Beard, T. W. McLain, D. B. Nelson, D. Kingston, and D. Johanson, "Decentralized Cooperative Aerial Surveillance Using Fixed-Wing Miniature UAVs," *Proceedings of the IEEE,* vol, 94, pp. 1306-1324, 2006.

[52] W. Ren and R. W. Beard, "Consensus Seeking in Multi-Agent Systems under Dynamically Changing Interaction Topologies," *IEEE Transactions on Automatic Control,* vol. 50, pp. 655-661, 2004.

[53] J. Cheong, S.-I. Niculescu, A. Annaswamy, and M. A. Srinivasan, "Synchronization Control for Physics-based Collaborative Virtual Environments with Shared Haptics," *Advanced Robotics,* vol. 21, pp. 1001-1029, 2007.

[54] S.-I. Niculescu and A. M. Annaswamy, "An Adaptive Smith-Controller for Time-delay Systems with Relative Degree $n* >= 2$," *Systems and Control Letters,* vol. 49, pp. 347-358, 2003.

[55] L. Crocco, "Aspects in Combustion Stability in Liquid Propellant Rocket Motors, Part I: Fundamentals - Low Frequency Instability with Monopropellants," *Journal of American Rocket Society,* vol. 21, pp. 163-178, 1951.

[56] M. Bozorg and E. J. Davison, "Control of Time Delay Processes with Uncertain Delays: Time Delay Stability Margins," *Journal of Process Control,* vol. 16, pp. 403-408, 2006.

[57] N. Olgac and B. T. Holm-Hansen. "A Novel Active Vibration Absorption Technique: Delayed Resonator," *Journal of Sound and Vibration,* vol. 176, pp. 93-104, 1994.

[58] Z. N. Masoud N. and A. H. Nayfeh, "Sway Reduction on Container Cranes Using Delayed Feedback Controller." *Nonlinear Dynamics,* vol. 34, pp. 347-358, 2003.

[59] Richard, J.P., "Time-Delay Systems: an Overview of Some Recent Advances and Open Problems," *Automatica*, vol. 39, pp. 1667-1694, 2003.

[60] L. E. El'sgol'ts and S. B. Norkin, *Introduction to the Theory and Applications of Differential Equations with Deviating Arguments.* Academic Press, New York, 1973.

[61] C. Foley and M. C. Mackey, "Dynamic Hematological Disease: A Review," *Journal of Mathematical Biology,* vol. 58, pp. 285-322, 2009.

[62] K. L. Cooke and P. van den Driessche, "On Zeroes of Some Transcendental Equations," in *Funkcialaj Ekvacioj,* vol. 29, pp. 77-90, 1986.

[63] A. Callender, D. R. Hartree, and A. Porter, "Time Lag in a Control System," *Philosophical Transactions of Royal Society London Series A, Mathematical and Physical Sciences,* vol. 235, pp. 415-444, 1936.

[64] A. Callender and A. G. Stevenson, "The Application of Automatic Control to a Typical Problem in Chemical Industry,". *Society of Chemical Industry,* vol. 18, pp. 108-116, 1936.

[65] Editorial Staff, "The Damping Effect of Time Lag," *Engineer,* vol. 163, pp. 439, 1937.

[66] M. S. Lee and C. S. Hsu, "On the τ-Decomposition Method of Stability Analysis for Retarded Dynamical Systems," *SIAM Journal on Control,* vol. 7, pp. 242-259, 1969.

[67] J. Neimark, "D-Subdivisions and Spaces of Quasi-Polynomials," *Prikl. Mat. Meh.*, vol. 13, pp. 349-380, 1949.

[68] N. Olgac and R. Sipahi, "An Exact Method for the Stability Analysis of Time-Delayed LTI Systems," *IEEE Transactions on Automatic Control,* vol. 47, pp. 793-797, 2002.

[69] J. Louisell, "Absolute Stability in Linear Delay-Differential Systems: Ill-Possedness and Robustness," *IEEE Transactions on Automatic Control,* vol. 40, pp. 1288-1291, 1995.

[70] Z. V. Rekasius, "A Stability Test for Systems with Delays," *Proc. 1980 Joint Automatic Control Conference.*, San Francisco, CA, 1980, article no. TP9-A.

[71] O. Toker and H. Özbay, "Complexity Issues in Robust Stability of Linear Delay-Differential Systems," *Mathematics of Control, Signals, and Systems*, vol. 9, pp. 386-400, 1996.

[72] J. Chiasson, Z. Tang, J. Ghanem, C. T. Abdallah, J. D. Birdwell, M. M Hayat, and H. Jerez, "The Effects of Time Delay Systems on the Stability of Load Balancing Algorithms for Parallel Computations," *IEEE Transactions on Control Systems Technology,* vol. 13, pp. 932-942, 2005.

[73] R. Izmailov, "Analysis and Optimization of Feedback Control Algorithms for Data Transfers in High-Speed Networks," in *SIAM Journal on Control and Optimization,* vol. 34, pp. 1767-1780, 1996.

[74] S.-I. Niculescu, "On Delay Robustness Analysis of a Simple Control Algorithm in High-Speed Networks," *Automatica*, vol. 38, pp. 885-889, 2002.

[75] N. Olgac and R. Sipahi, "A Unique Methodology for Chatter Stability Mapping in Simultaneous Machining," *ASME Journal of Manufacturing Science and Engineering,* vol. 127, pp. 791-800, 2005.

[76] J. Chen, P. Fu, and S.-I. Niculescu, "When will Zeros of Time-Delay Systems Cross Imaginary Axis?" *Proc. European Control Conference*, Kos, Greece, 2007, pp. 5631-5638.

[77] H. Fazelinia, R. Sipahi, and N. Olgac, "Stability Analysis of Multiple Time Delayed Systems Using 'Building Block' Concept," *IEEE Transactions on Automatic Control,* vol. 52, pp. 799-810, 2007.

[78] R. Sipahi and N. Olgac, "Complete Stability Map of Third Order LTI Multiple Time Delay Systems," *Automatica,* vol. 41, pp. 1413-1422, 2005.

[79] C. Abdallah, P. Dorato, J. Benitez-Read, and R. Byrne, "Delayed Positive Feedback can Stabilize Oscillatory Systems," *Proc. American Control Conference,* San Francisco, CA, 1993, pp. 3106-3107.

[80] K. Engelborghs, T. Luzyanina, and G. Samaey, *DDE-BIFTOOL v. 2.00: a Matlab Package for Bifurcation Analysis of Delay Differential Equations,* TW Report 330, Department of Computer Science, Katholieke Universiteit Leuven, Belgium, October 2001. `http://twr.cs.kuleuven.be/research/software/delay/ddebiftool.shtml`

[81] R. Sipahi and N. Olgac, "Stability Robustness of Retarded LTI Systems with Single Delay and Exhaustive Determination of Their Imaginary Spectra," *SIAM Journal on Control and Optimization,* vol. 45, pp. 1680-1696, 2006.

[82] J. J. Craig, P. Hsu, and S. S. Sastry, "Adaptive Control of Mechanical Manipulators," *International Journal of Robotics Research*, vol. 6, pp. 16-28, 1987.

[83] V. L. Kharitonov, S.-I. Niculescu, J. Moreno, and W. Michiels, "Static Output Feedback Stabilization: Necessary Conditions for Multiple Delay Controllers," *IEEE Transactions on Automatic Contrl.*, vol. 50, pp. 82-86, 2005.

[84] H. Kokame, K. Hirata, K. Konishi, and T. Mori, "Difference Feedback can Stabilize Uncertain Steady States," *IEEE Transactions on Automatic Control,* vol. 46, pp. 1908-1913, 2001.

[85] G. Meinsma, M. Fu, and T. Iwasaki, "Robustness of the Stability of Feedback Systems with Respect to Small Time Delays," *Systems and Control Letters,* vol. 36, pp. 131-134, 1999.

[86] T. Heil, I. Fischer, W. Elsäßer, B. Krauskopf, K. Green, and A. Gavrielides, "Delay Dynamics of Semiconductor Lasers with Short External Cavities: Bifurcation Scenarios and Mechanisms," *Physical Review E,* vol. 67, article no. 066214, 2003.

[87] W. Michiels, "Stability Analysis of Oscillatory Systems Subject to Large Delays: A Synchronization Point of View," *Journal of Vibration and Control,* vol. 16, pp. 1087-1111, 2010.

[88] P. Freitas, "Delay-Induced Instabilities in Gyroscopic Systems," *SIAM Journal on Control and Optimization*, vol. 39, pp. 196-207, 2000.

[89] R. H. Middleton and D. E. Miller, "On the Achievable Delay Margin Using LTI Control for Unstable Plants," *IEEE Transactions on Automatic Control,* vol. 52, pp. 1194 - 1207, 2007.

[90] F. Mazenc, S. Mondie, and S.-I. Niculescu, "Global Asymptotic Stabilization for Chains of Integrators with a Delay in the Input," *IEEE Transactions on Automatic Control,* vol. 48, pp. 57-63, 2003.

[91] J. Moreno, "An Extension of Lucas Theorem to Entire Functions," *Proc. 1st IFAC Workshop on Linear Time-Delay Systems,* Grenoble, France, 1998. Available at `http://www.ifac-papersonline.net/`

[92] K. Gu, S.-I. Niculescu, and J. Chen, "On Stability of Crossing Curves for General Systems with Two Delays," in *Journal of Mathematical Analysis and Applications*, vol. 311, pp. 231-253, 2005.

[93] E. Jarlebring, "Critical Delays and Polynomial Eigenvalue Problems," *Journal of Computational and Applied Mathematics,* vol. 224, pp. 296-306, 2009.

[94] A. F. Ergenc, N. Olgac, and H. Fazelinia, "Extended Kronecker Summation for Cluster Treatment of LTI Systems with Multiple Delays," *SIAM Journal on Control and Optimization,* vol. 46, pp. 143-155, 2007.

[95] S. Yi, P. W. Nelson, and A. G. Ulsoy, "Delay Differential Equations via the Matrix Lambert W Function and Bifurcation Analysis: Application to Machine Tool Chatter," *Mathematical Biosciences and Engineering,* vol. 4, pp. 355-368, 2007.

[96] T. Kalmar-Nagy, G. Stepan, and F. C. Moon, "Subcritical Hopf Bifurcation in the Delay Equation Model for Machine Tool Vibrations," *Nonlinear Dynamics,* vol. 26, pp. 121-142, 2001.

[97] N. MacDonald, "An Interference Effect of Independent Delays," *IEE Proceedings of Control Theory & Applications, Pt. D,* vol. 134, pp. 38-42, 1987.

[98] W. Michiels and S.-I. Niculescu, "Characterization of Delay-Independent Stability and Delay-Interference Phenomena," *SIAM Journal on Control and Optimization*, vol. 45, pp. 2138-2155, 2007.

[99] R. Datko, "Time Delay Perturbations and Robust Stability," in *Differential Equations, Dynamical Systems, and Control Science.* LNM, Marcel Dekker, New York, vol. 152, pp. 457-468, 1994.

[100] Ya. Z. Tsypkin, "The systems with Delayed Feedback," in *Avtomathika i Telemech.,* vol. 7, pp. 107-129, 1946.

[101] J. K. Hale, E. F. Infante, and F. S.-P. Tsen, "Stability in Linear Delay Equations," in *Journal of Mathematical Analysis and Applications.*, vol. 105, pp. 533-555, 1985.

[102] Z. J. Palmor, "Time-Delay Compensation – Smith Predictor and its Modifications," in *The Control Handbook*, W.S. Levine (Eds.), CRC Press, pp. 224-237, 1996.

[103] I. Horowitz, "Some Properties of Delayed Controls (Smith Regulators)," *International Journal of Control,* vol. 38, pp. 977-990, 1983.

[104] C.-I. Morărescu, S.-I. Niculescu, and K. Gu, "On the Geometry of Stability Regions of Smith Predictors Subject to Delay Uncertainty," *IMA Journal of Mathematical Control and Information,* vol. 24, pp. 411-423, 2007.

[105] Zhong, Q.-C., *Robust Control of Time-delay Systems.* Springer, 2006.

[106] R. Sipahi and N. Olgac, "Stability Map of Systems with Three Independent Delays," *Proceedings of the American Control Conference,* Minneapolis, MN, 2006, pp. 2451-2456.

[107] K. Gu and M. Naghnaeian, "On Stability Crossing Set for General Systems with Three Delays—Part 1. and Part 2," *8th IFAC Workshop on Time Delay Systems*, Sinaia, Romania, 2009. Available at `http://www.ifac-papersonline.net/`.

[108] R. Sipahi, S. Lammer, D. Helbing, and S.-I. Niculescu, "On Stability Problems of Supply Networks Constrained with Transport Delay," *ASME Journal of Dynamic Systems, Measurement & Control,* vol 131, article no. 021005, 2009.

[109] R. Sipahi and I.I. Delice, "Extraction of 3D Stability Switching Hypersurfaces of a Time Delay System with Multiple Fixed Delays," *Automatica*, vol. 45, pp. 1449-1454, 2009.

[110] A.A. Khan, D.M. Tilbury, and J. R. Moyne, "Favorable Effect of Time Delays on Tracking Performance of Type-I Control Systems," *IET Control Theory & Applications*, vol. 2, pp. 210-218, 2008.

[111] M. Casgadli, "A Dynamical Systems Approach to Modeling Input-Output Systems," in *Nonlinear Modeling and Forecasting.* M. Casgaldi and S. Eubank (Eds.), Proc. vol. XII, Santa Fe Institute Studies in the Sciences of Comlexity, Addison-Wesley, Redwood City, CA, 1992, pp. 265–281.

[112] M. El Moursi, G. Joos, and C. Abbey, "A Secondary Voltage Control Strategy for Transmission Level Interconnection of Wind Generation," *IEEE Transactions on Power Electronics,* vol. 23, pp. 1178-1190, 2008.

[113] J. He, C. Lu, X. Wu, P. Li, J. Wu, "Design and Experiment of Wide Area HVDC Supplementary Damping Controller Considering Time Delay in China Southern Power Grid," *IET Generation, Tranmission and Distribution*, vol. 3, pp. 17-25, 2009.

[114] K. Tomsovic, D. E. Bakken, V. Venkatasubramanianm, A. Bose, "Designing the Next Generation of Real-Time Control, Communication, and Computations for Large Power Systems," *Proceddings of the IEEE*, vol. 93, pp 965-979, 2005.

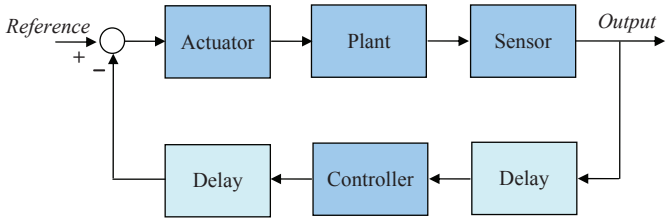

Figure 1: Delays in a feedback system. Feedback control systems often function in the presence of delays, primarily due to the time it takes to acquire the information needed for decision-making, to create the control decisions, and to execute these decisions.

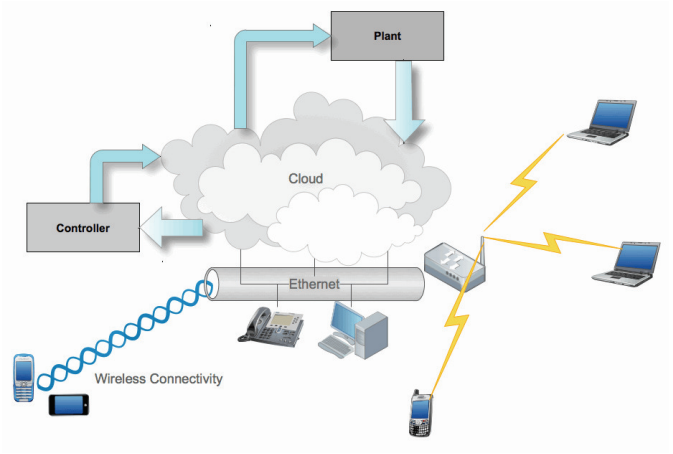

Figure 2: Network control systems. Controlling across a shared communication network is a challenging task due to the delays arising in the communication medium. Delays can manifest themselves in the control signals, in the measured signals, and in external inputs traveling from their source to their destination through the links of the network.

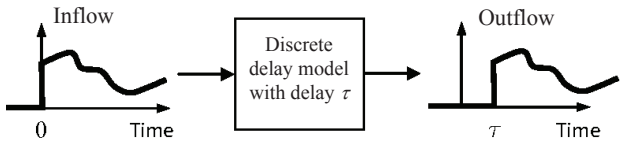

Figure 3: Constant delay model. Delay can be modeled as a buffer that holds the inflow signal for a length of time, then releases the signal without distortion. This type of delay represents a first-in-first-out-type model found in sensing, information transmission, and mass transport.

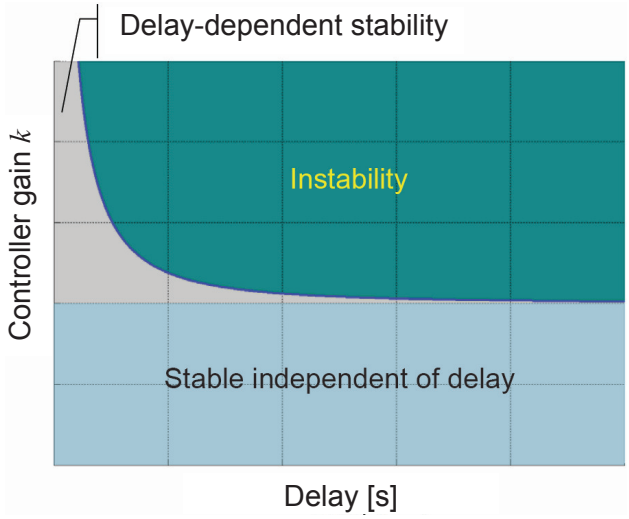

Figure 4: Stability chart. This chart is obtained for a closed-loop system with the plant transfer function $e^{-\tau s}b/(s+a)$ and the controller $C(s) = k$. This stability chart is partitioned into three regions, namely, the delay-independent stable region, the delay-dependent stability region, and the unstable region. This chart reveals the effect of a delay parameter on stability, and how the controller gain k can be tuned to avoid instability.

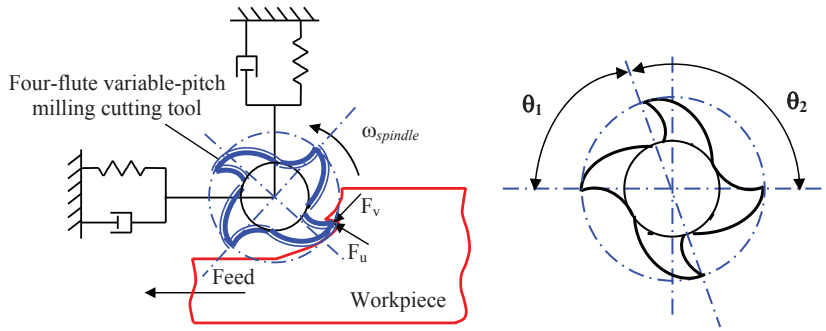

(a) ***Milling operation.*** **(b)** ***Four-flute variable-pitch cutting tool.***

Figure 5: Variable-pitch milling. A four-flute cutting tool with pitch angles θ_1 and θ_2 is used to machine a metal workpiece. Due to the flexibility of the tool, each tooth leaves some uncut material that is encountered by the next tooth as an additional force. That is, a past event affects the evolution of the cutting dynamics. The delays that arise from this mechanism are proportional to the tooth-passing period.

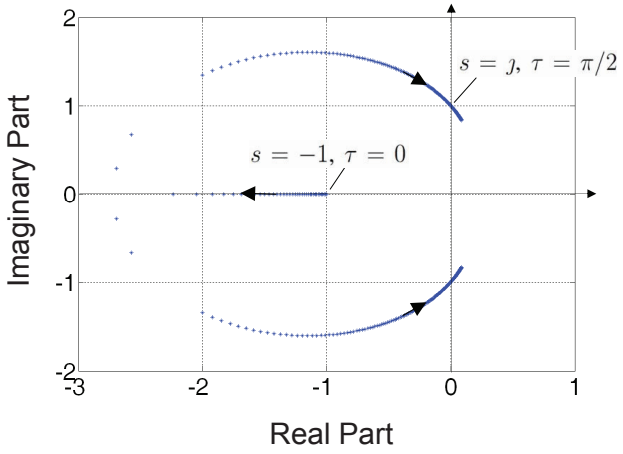

Figure 6: Rightmost characteristic roots on the complex plane. Location of the rightmost characteristic roots of the closed-loop system with the characteristic equation $s+ke^{-s\tau} = 0$ for various values of $\tau \in [0, 2]$ with $k = 1$. For $\tau = \pi/(2k)$, the rightmost root crosses toward the right-half plane causing instability. The rightmost roots are computed using DDE-BIFTOOL, which is a numerical bifurcation tool developed for delay differential equations [80].

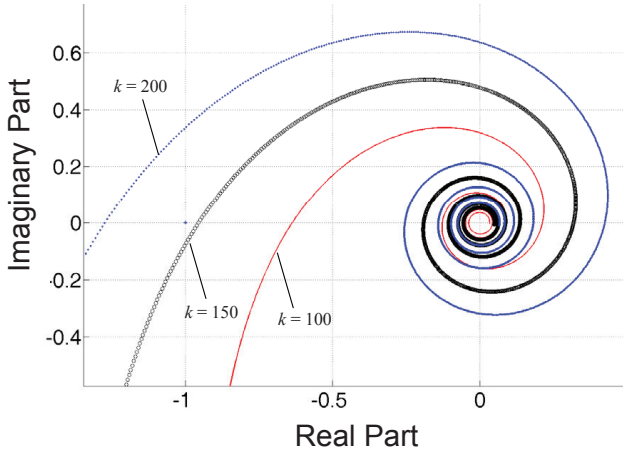

Figure 7: Nyquist plot for several controller gains k. The plot depicts the Nyquist plot of a closed-loop control system with the transfer function $H(s) = 1/s$ and the proportional feedback control law $C(s) = -ke^{-\tau s}$ with delay $\tau = 0.01$ s.

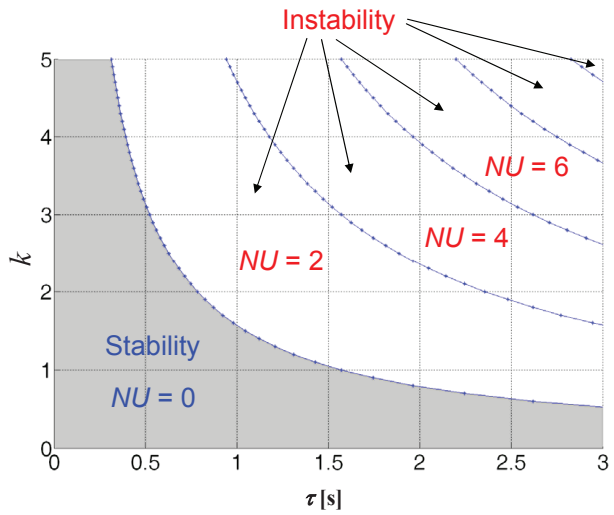

Figure 8: Stability chart with respect to the delay τ and controller gain k. The plot depicts the stability chart of a closed-loop system with the transfer function $H(s) = 1/s$ and the control law $C(s) = -ke^{-\tau s}$, where $0 \leq k \leq 5$. Each pair $(\tau\,, k)$ selected from the shaded region leads to stability of the control system. If, for a given pair $(\tau\,, k)$, the system is stable, then the number NU of unstable roots is zero.

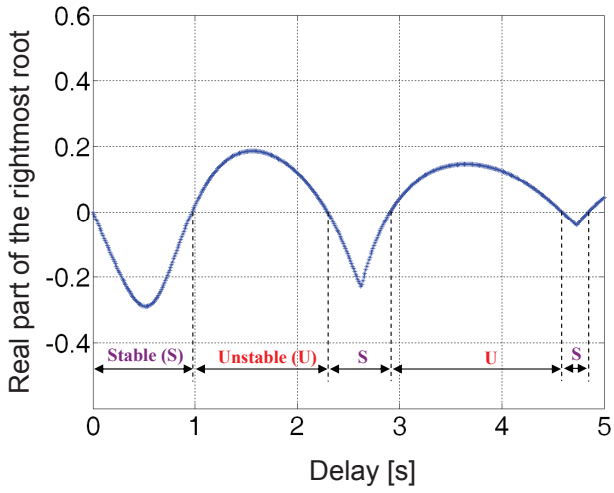

Figure 9: Behavior of the real part of the rightmost root. For a closed-loop system with the characteristic equation $f(s;\tau) = s^2 + 9 - 1.5\,e^{-\tau s} = 0$, this plot depicts how the real part of the rightmost characteristic root behaves with respect to the delay parameter τ. The sign change of the real part indicates how the closed-loop system switches from stability to instability several times.

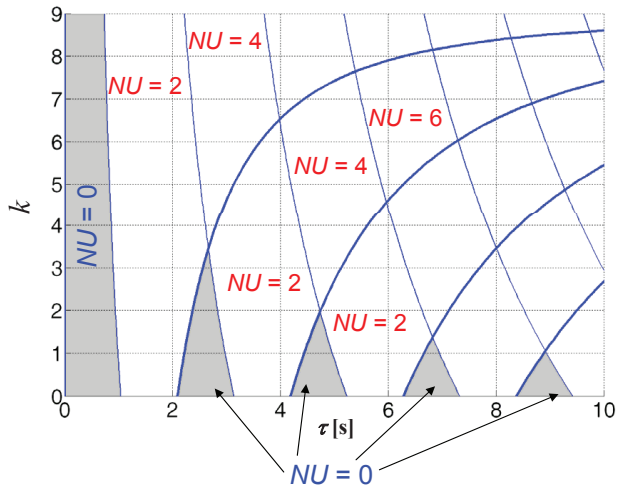

Figure 10: Stability chart with respect to the delay τ and controller gain k. This plot depicts the stability chart of a closed-loop control system with the transfer function $H(s) = 1/(s^2 + \omega_0^2)$ and the control law $C(s) = ke^{-\tau s}$, where $\omega_0 = 3$ and $0 < k < 9$. Each pair $(\tau\,, k)$ selected from the shaded regions leads to stability of the control system, that is, the number NU of unstable roots is zero.

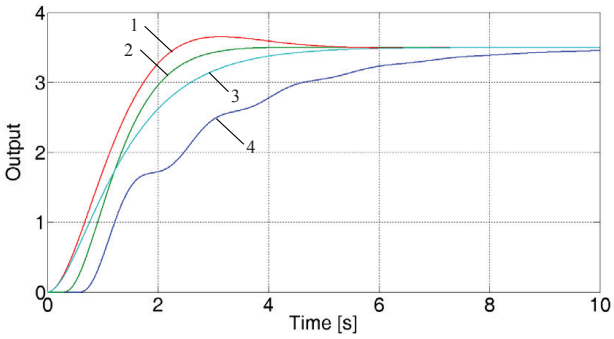

Figure 11: Unit step response. The positive feedback control loop consists of the open-loop transfer function $H(s) = 1/(s^2 + 9)$ and the controller $C(s) = (k_p e^{-\tau s} + k_d s)$. The aim is to compare the speed of response between a delay-free proportional-derivative controller ($k_p \neq 0$, $k_d \neq 0$, $\tau = 0$) and a delayed proportional controller ($k \neq 0$, $\tau \neq 0$). Curve 1 denotes the case where there is no delay in the closed-loop system with the controller gains $k_p = 7$ and $k_d = -2$. Curve 2 corresponds to the output of the system with $\tau = 0.3$ s and the proportional controller gain $k = 7$. Curve 3 represents the output of the system where there is no delay, and the controller gains are selected as $k_p = 7$ and $k_d = -3$. Finally, curve 4 denotes the output of the system where the delay is $\tau = 0.6$ s and the controller gain is $k = 7$.

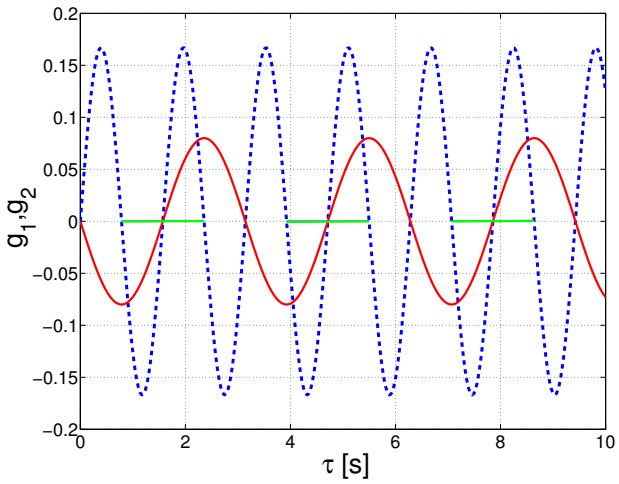

Figure 12: Verification of stable poles. Using the sinusoidal functions in (25), the location of the poles in the complex plane can be determined. The sign agreement between g_1 and g_2 indicates that the closed-loop system is stable. This example shows that stability can be deduced from the phase synchronization of two functions g_1 and g_2 derived from the characteristic equation of the system.

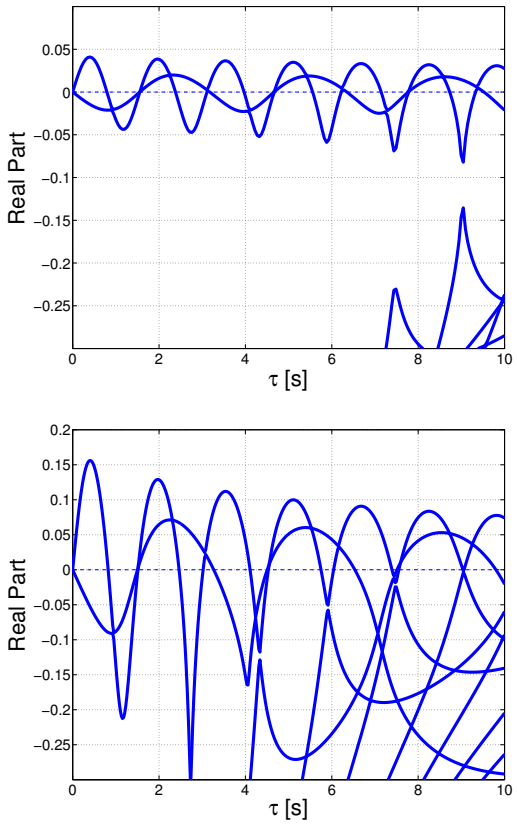

Figure 13: Rightmost root distributions of (24). The curves in both panels show how the real part of the rightmost roots of the characteristic equation (24) vary with respect to the delay τ, where $\omega_1 = 2$ and $\omega_2 = 4$. The left and right panels correspond to $\varepsilon = 1/4$ and $\varepsilon = 1$ in the numerical example, respectively.

	0	1	2	3	4	5	$\text{card}(\mathcal{S}_+)$
1	/	/	/	/	/	/	
2	/	/	Condition (37)				
3	/	/	/	/	/	/	
4	/	/	/	/			
5	/	/	/	/	/	/	
6	/	/	/	/	/	/	
$\text{card}(\mathcal{U}_+)$							

Table 1: Limitations of output feedback stabilizability when using the delay as a controller parameter. Necessary and sufficient stabilizability conditions are given by Proposition 4 in terms of two measures, namely, $\text{card}(\mathcal{S}_+)$ and $\text{card}(\mathcal{U}_+)$, where $\text{card}(\mathcal{S}_+)$ is the number of unstable closed-loop poles, and $\text{card}(\mathcal{U}_+)$ is the number of distinct crossing frequencies that the system's imaginary poles can create for some delay τ. The symbol "/" means that stabilization is not possible. For the case $(\text{card}(\mathcal{U}_+), \text{card}(\mathcal{S}_+))$ equal to either $(2, 2)$ or $(2, 3)$, all stabilizing delay values are described by condition (37).

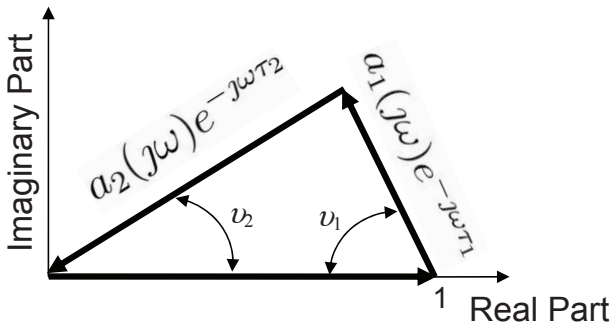

Figure 14: Geometric interpretation of (43). Equation (43) is represented in the complex plane as the sum of three vectors. If these vectors create a triangle in the complex domain, then the characteristic equation has a solution at $s = j\omega$ for some delays τ_1 and τ_2. For all delay values, since the norms of the vectors are independent of the delays, we can write conditions, called *triangle inequalities*, for a triangle to form on the complex plane. Inequality conditions are in terms of only ω, and require that the length of each edge of a triangle cannot exceed the sum of the lengths of the remaining two edges. Once all ω satisfying these triangle conditions are detected, the delays τ_1 and τ_2 can be calculated using ω and the orientation of the vectors.

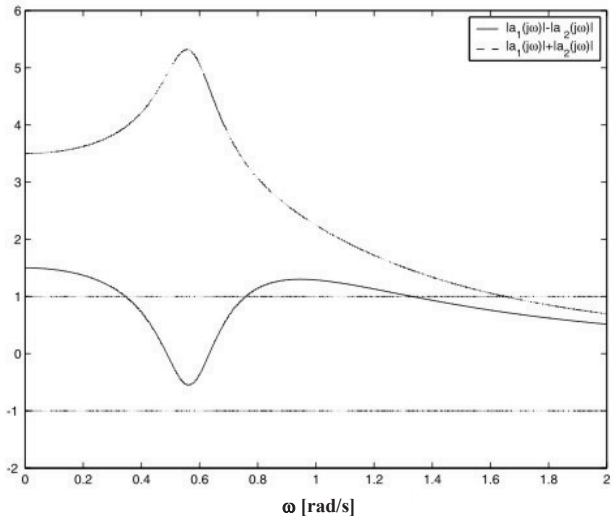

Figure 15: Frequency-sweeping test. By sweeping the frequency ω, the norm $|a_1(\jmath\omega)| \pm |a_2(\jmath\omega)|$ is visualized as a function of ω for the system (46) and (47). This plot yields the range of frequencies for which the triangle conditions (44)-(45) hold. These frequency ranges generate the delay solutions τ_1-τ_2 in Figure 16 and Figure 17. Reprinted with permission from Elsevier. See [92] for full citation.

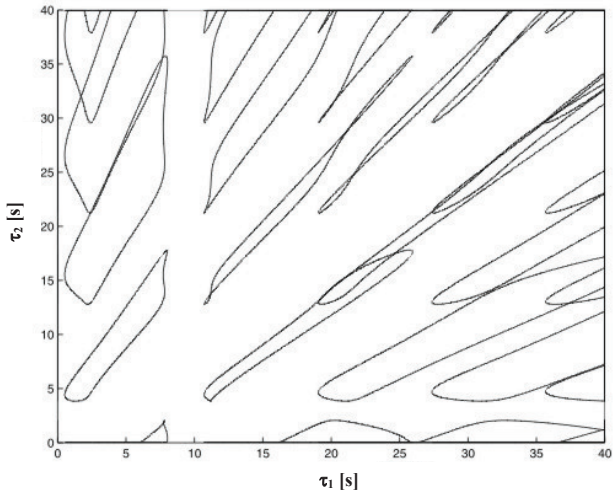

Figure 16: Delay solutions on closed curves. The curves $\mathcal{C}_1$ of the system in Example 6 are the stability-switching curves, which represent the delay values with which the characteristic equation has a pair of roots on the imaginary axis. These curves decompose the delay plane into regions in which all delays lead to the same number NU of unstable roots of the system. Reprinted with permission from Elsevier. See [92] for full citation.

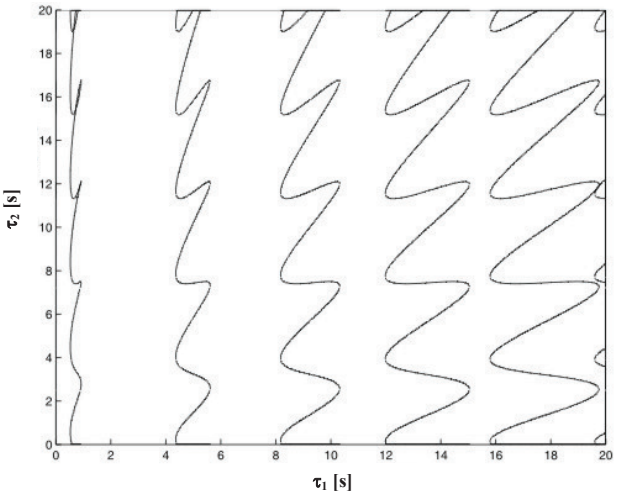

Figure 17: Delay solutions on open-ended spirals. The curves $\mathcal{C}_2$ of the system in Example 6 are the stability-switching curves, which represent the delay values with which the characteristic equation has a pair of roots on the imaginary axis. These curves decompose the delay plane into regions in which all delays lead to the same number NU of unstable roots. Reprinted with permission from Elsevier. See [92] for full citation.

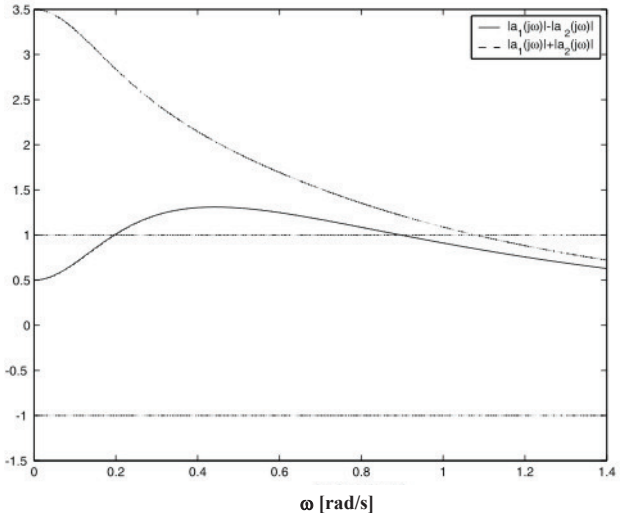

Figure 18: Frequency-sweeping test. By sweeping the frequency ω, the norm $|a_1(\jmath\omega)| \pm |a_2(\jmath\omega)|$ is visualized as a function of ω for the system (48) and (49). This plot yields the range of frequencies for which the triangle conditions (44)-(45) hold. These frequency ranges generate the delay solutions τ_1-τ_2 in Figure 19. Reprinted with permission from Elsevier. See [92] for full citation.

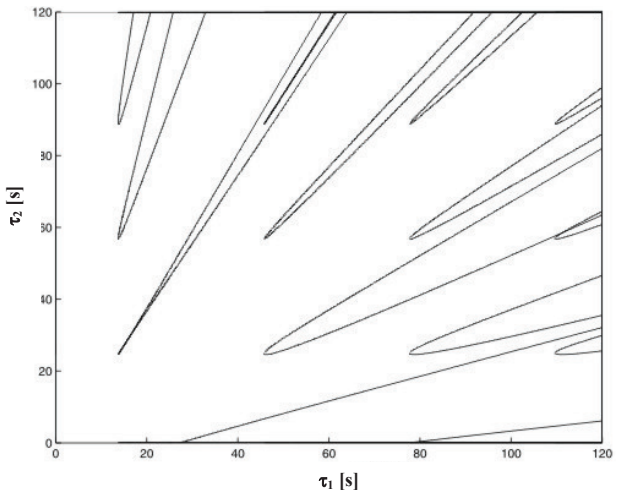

Figure 19: Delay solutions on open-ended curves. The delay pairs in the τ_1-τ_2 plane lead to either stability or instability. The boundaries separating the stability and instability regions are determined by the stability-switching curves of the system. In the example (48), (49), these curves are in the form of open-ended forms. Reprinted with permission from Elsevier. See [92] for full citation.

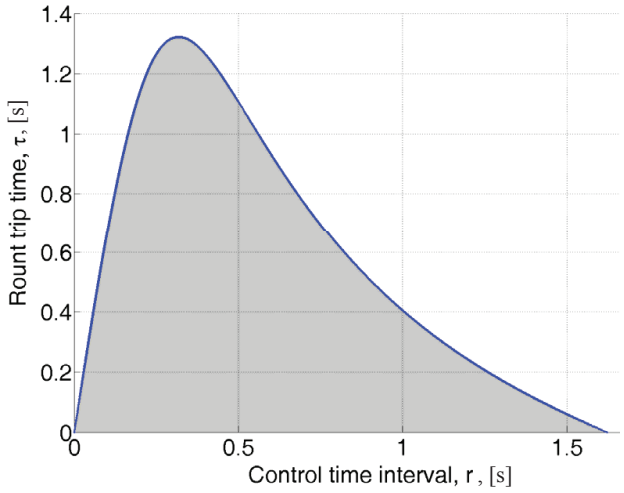

Figure 20: Stability chart. The shaded regions in the delay-parameter space $(\tau\,, r)$ represent the stability regions of the congestion control model (50). The delay $r \neq 0$, which is the control-time interval, can be chosen to guarantee stability for a round-trip time as large as $\tau \approx 1.3$ s.

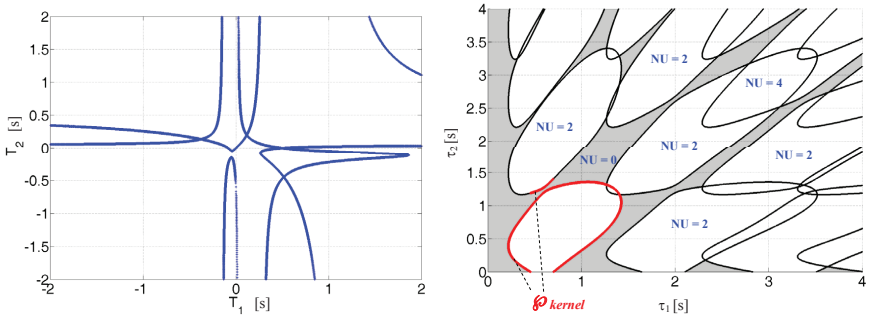

(a) ***Parametric domain in*** (T_1, T_2)**.** **(b)** ***Delay domain*** (τ_1, τ_2)**.**

Figure 21: Mapping from the parametric domain (T_1, T_2) to the delay domain (τ_1, τ_2). The domain (T_1, T_2) is used to detect the stability-switching curves (SSC) in the delay domain. These curves are essential for the stability analysis since they determine the boundaries that separate stability from instability in the delay domain. To find SSC, the points (T_1, T_2) that create imaginary roots $s = \jmath\omega$ in (54) are crucial. In panel (a), these points are depicted for this numerical example. Next, using the triplets (ω, T_1, T_2), SSC can be obtained from (53) as shown in panel (b). In panel (b), the stability regions in the delay domain are shaded, the number NU of unstable roots is shown, and the kernel curve is marked. In this stability analysis, we see that multiple disjoint stability regions arise, offering several choices to select or schedule the delays in the closed-loop system in a way to stabilize the system.

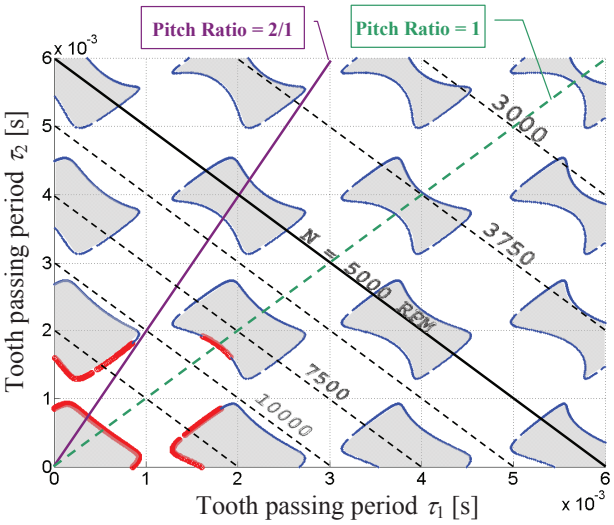

Figure 22: Stability chart of the metal-cutting dynamics. The gray shaded regions show the parametric selections corresponding to stability, which refers to machining with vibration-free engagement of the cutting tool with the workpiece. The ratio τ_2/τ_1 corresponds to the pitch ratio of the cutting tool, while the lines with slopes -1 correspond to the rotational speed of the spindle in revolutions per minute, which can be chosen appropriately to render stable cutting dynamics, thereby avoiding undesirable vibration at the interface between the cutting tool and the workpiece.

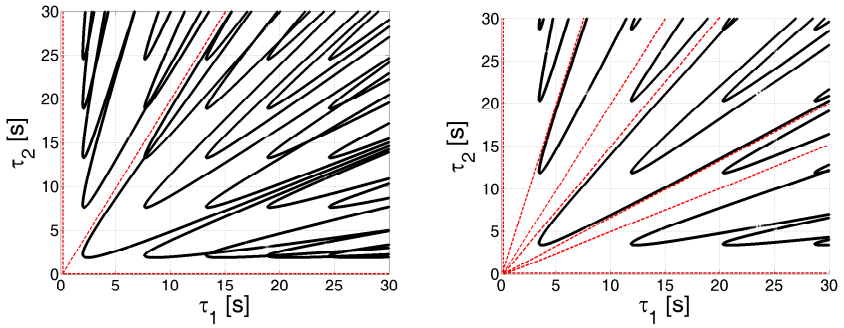

Figure 23: Investigation of delay interference. Stability and instability regions of (59) are presented in the (τ_1, τ_2)-space for $a = 1$ (left) and $a = 1.3$ (right). For $a = 1$, three stable rays, two of which are the axes, exist. If $a = 1.3$, then the number of rays including the axes is seven. These rays, which are shown with dashed lines, define all combinations of multiple delays for which the closed-loop system remains stable. That is, the system is stable independently of the delays that lie on these rays. When constructing controllers, the existence of such rays can be useful, but the control designer needs to pay attention to avoid instability when the slopes of these rays are perturbed due to uncertainty in the delays.

7 Sidebar 1: Notation

In this article, we use $s \in \mathbb{C}$ for the Laplace variable; $\Re(s)$ for the real and $\Im(s)$ for the imaginary part of s; $\mathbb{R}_+$, $\mathbb{R}_-$, $\mathbb{Z}_+$, and $\mathbb{Z}_{0,+}$ denote the set of positive real numbers, negative real numbers, positive integers, and nonnegative integers, respectively. The notation $\sup(\cdot)$ stands for the supremum of $(\cdot)$; $\lfloor(\cdot)\rfloor$ for the floor of $(\cdot)$; det for the determinant of a square matrix; $\dot{x}(t) = dx/dt$ for the time derivative of x; $\jmath$ for the imaginary number; $\jmath\mathbb{R}$ for the imaginary axis; $\mathbb{C}_-$ and $\mathbb{C}_+$ for the open left half and open right half of the complex plane, respectively; $\bar{\mathbb{C}}_+$ for the closed right half of the complex plane; τ denotes a delay, and $\vec{\tau} = \{\tau_\ell\}_{\ell=1}^{L}$ is the set whose elements are the scalar delays τ_ℓ.

8 Sidebar 2: Delays in Microscopic Vehicular Traffic Flow

Human drivers have reaction delays, that is, drivers need a minimal amount of time to become aware of external events and make decisions. Vehicular traffic is thus affected by delays [1, S1]. Reaction delays vary under physical conditions and stimuli, and depends on the drivers' cognitive and physiological states. Experimental and simulator measurements indicate that these delays range between 0.6 s and 2 s. Not only do delays invite collisions, but delays can also cause traffic jams and stop-and-go waves, making traffic prone to slinky-type instabilities. These effects contribute to casualties on highways, increased emissions due to jams, and productivity losses due to increased travel times [S1–S3].

Numerous approaches of varying complexity are used to model vehicular traffic flow [1, S1]. One option is to assume that the vehicles follow each other in a single lane as shown in Figure S1. The resulting models are at a microscopic level, which allows the inclusion of human reaction delays.

We now present three models to explain the ideas behind deriving traffic-flow models. The first model with delay is given by

$$\ddot{x}_i(t) = \kappa \left(\dot{x}_{i+1}(t-\tau) - \dot{x}_i(t-\tau) \right), \tag{S1}$$

where $i = 1, \ldots, n$, and n is the number of vehicles. In (S1), the terms $\ddot{x}_i$ and $\dot{x}_i$ are, respectively, the acceleration and velocity perturbations of vehicle i around a constant vehicle velocity v. In this model, κ is a positive constant, and the delay τ is the driver reaction delay. The stability of (S1) is studied in the delay-free case [S4, S5], as well as in the presence of delay τ [S6]. Analytical predictions obtained from (S1) tend to match experiments performed with human drivers [1]. Stability analysis of this model can further be used to analyze the flow characteristics of traffic, how traffic jams occur, and how human driving affects these jams. This analysis is related to how traffic impacts the environment and the economy.

The second model is given by

$$\ddot{x}_i(t) = \kappa \left[V(\Delta_i(t-\tau)) - \dot{x}_i(t-\tau) \right], \tag{S2}$$

where τ is the driver's reaction delay, the headway $\Delta_i(t) = x_{i+1}(t) - x_i(t)$ is the distance between vehicles i and $i+1$, and $V(\Delta_i(t))$ is the *optimal velocity function*, which determines how a vehicle can cruise faster so long as it maintains larger headway with respect to the preceding vehicle [S7]. Optimal

velocity functions can be identified based on experimental measurements [S7–S9].

The third model presented considers the case where drivers observe multiple vehicles ahead [4, S10]. This driving strategy modifies (S1) as

$$\ddot{x}_i(t) = \sum_{p=1}^{N_i} \kappa_{p,i} \left(\dot{x}_{i+p}(t - \tau_{p,i}) - \dot{x}_i(t - \tau_{p,i}) \right), \tag{S3}$$

where $\kappa_{p,i}$ is a constant penalizing the velocity perturbation differences between the i^{th} and $(i+p)^{th}$ vehicle sensed with delay $\tau_{p,i}$, and $N_i > 1$ is the number of vehicles that the i^{th} vehicle is following. In this case, multiple delays can represent a driver's sensing time of different vehicles.

References

[S1] D. Helbing, "Traffic and Related Self-Driven Many-Particle Systems," *Reviews of Modern Physics,* vol. 73, pp. 1067-1141, 2001.

[S2] R. Subramanian, "Motor Vehicle Traffic Crashes as a Leading Cause of Death in the United States, 2005," Traffic Safety Facts, Research note, National Highway Traffic Safety Administration (NHTSA), 2008. Available at `http://www-nrd.nhtsa.dot.gov/Pubs/810936.PDF`.

[S3] G. Orosz, E. Wilson, and G. Stépán (Eds.), "Traffic jams: dynamics and control," *Philosophical Transactions of the Royal Society A,* vol. 368, 2010.

[S4] A. Reuschel, "Fahrzeugbewegungen in der Kolonne," *Oesterreichisches Ingenieur-Archiv,* vol. 4, pp. 193-215, 1950.

[S5] A. Reuschel, "Fahrzeugbewegungen in der Kolonne bei gleichformig beschleunigtem oder verzogertem Leitfahrzeug," *Zeitschrift des Oesterreichischen Ingenieurund Architekten Vereines,* vol. 95, no. 7/8 pp. 59-62, no. 9/10 pp. 73-77, 1950.

[S6] R. E. Chandler, R. Herman, and E. W. Montroll, "Traffic Dynamics: Analysis of Stability in Car Following," *Operational Research,* vol.7, pp. 165-184, 1958.

[S7] M. Bando, K. Hasebe, K. Nakanishi, and A. Nakayama, "Analysis of Optimal Velocity Model with Explicit Delay," *Physical Review E,* vol. 58, pp. 5429-5435, 1998.

[S8] Y. Sugiyama and H. Yamada, "Simple and Exactly Solvable Model for Queue Dynamics," *Physical Review E,* vol. 55, pp. 7749-7752, 1997.

[S9] G. Orosz and G. Stepan, "Subcritical Hopf bifurcations in a Car-Following Model with Reaction-Time Delay," *Proceedings of the Royal Society of London A,* vol. 462, 2643-2670, 2006.

[S10] R. W. Rothery, "Transportation Research Board (Trb) Special Report 165," in *Traffic Flow Theory*, 2nd Edition, N. H. Gartner, C. J. Messner, and A. J. Rathi, Eds., 1998.

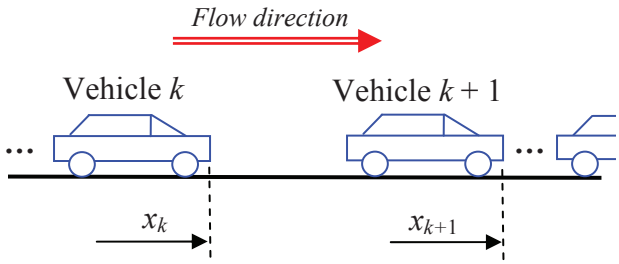

Figure S1: Platoon of vehicles. One way to model traffic flow is to assume that each driver follows a preceding vehicle without changing lanes. Human decision-making adds reaction delay to the flow dynamics. These delays, which are measured in the range of 0.6-2 s [2], affect the stability and flow characteristics of traffic, which in turn determine the impact of traffic on the environment and the economy.

9 Sidebar 3: Delays in Biology

The effects of neuromusculoskeletal torque generation on the stability of *quiet standing*, that is, maintaining the vertical configuration of the human body, can be investigated by means of experiments and analytical tools from control theory, see Figure S2 [19]. Quiet-standing experiments involve analyzing muscle activity at the ankles. Quiet standing is considered as an inverted pendulum controlled by the torque generated by muscles, and the torque created by the neuromusculoskeletal system. The torque due to the neuromusculoskeletal system is modeled by a critically damped system that receives input from a neural controller that creates corrective actions after the length of time τ.

A block diagram of the closed-loop quiet-standing system is shown in Figure S3, where the neural controller comprises a proportional-derivative controller with gains K_P and K_D, and where the mechanical controller is based on a damper-spring system defined by constants K and B. The effect of the torque created at the ankles on the deviation θ is felt after about 80-ms delay [19,S11,S12]. This delay is a combination of three different delays, namely, a delay of 40 ms for sensing the deviations θ, a delay of 27-37 ms in the cortex, and a delay of 3-13 ms for processing a decision.

Following the standard block diagram simplifications in Figure S3, we find the characteristic equation of quiet standing as

$$f(s; K_p, K_D, K, B) = Q_1(s, K_p, K_D, K, B) + e^{-\tau s} Q_2(s, K_p, K_D, K, B) = 0, \tag{S4}$$

where Q_1 and Q_2 are polynomials, and τ is the sensory delay of the human model. One goal is to find combinations of (K_p, K_D) such that the quiet-standing model (S4) is stable for a given delay τ. Additional applications at the intersection of neuroscience, control theory, and delay systems can be found in [S13].

9.1 Regulatory Networks

Cyclic biochemical feedback in cell regulatory networks is affected by delays. Consider the model

$$\dot{x}_1(t) = -\lambda_1 x_1(t) + c_1 x_2(t - \tau_1), \tag{S5}$$

$$\dot{x}_2(t) = -\lambda_2 x_2(t) + g(x_1(t - \tau_2)), \tag{S6}$$

where x_1 denotes the concentration of the messenger RNA (mRNA), x_2 denotes the concentration of the protein, which is the end product of the reaction, and the rate $\dot{x}(t)$ is defined by the balance between mRNA synthesis

and the end product consumption [S14]. The delays τ_1 and τ_2, respectively, define the lag from the initiation of the translation and from the initiation of the transcription until the appearance of the mature protein mRNA, $c_1 > 0$ describes the translation effects, $\lambda_1 > 0$ and $\lambda_2 > 0$ are related to degradation effects, and g is the feedback function.

System (S5)-(S6) is an example of a low-order biochemical oscillator model, where delays describe chemical or biochemical kinetics [S15–S19]. Delays are also encountered in mitogen-activated protein kinase cascades, which are reversible enzyme-activation-based mechanisms [S20]. These mechanisms are modeled as a series interconnections of compartments, which affect each other after a transport time of length τ_k, as shown in Figure S4. Circadian rhythm generators and dynamics of gene transcriptions are also examples of feedback control affected by delays [S21, S22].

9.2 Epidemics

Understanding the underlying mechanisms of biological processes and epidemics represents a challenge for health workers engaged in designing clinically relevant treatment strategies. These mechanisms can be revealed by considering epidemics and diseases as dynamical processes.

Hematology dynamics can be modeled by

$$\dot{x}(t) = -\lambda x(t) + G(x(t-\tau)), \tag{S7}$$

which formulates the circulating cell populations in one compartment, where x represents the circulating cell population, λ is the cell-loss rate, and the monotone function G, which describes a feedback mechanism, denotes the flux of cells from the previous compartment [61]. The delay τ represents the average length of time required to go through the compartment. The model (S7) is also found in population dynamics, where the delay represents a maturation period.

Models representing regulatory feedback mechanisms in the production of blood cells are similar to (S7). An example is the characteristic equation of the linearized system

$$f(s;\tau,\lambda,\lambda_E,k) = (s+\lambda)\left[(s+\lambda)(s+\lambda_E) + ke^{-s\tau}\right] = 0, \tag{S8}$$

where $\lambda > 0$ is the death rate, $\lambda_E > 0$ is the decay constant of a hormone at the equilibrium of the dynamics, and τ is the length of time needed for the maturation of red-blood-cell precursors [S23].

Examples are also found in the dynamics of *leukemia*, that is, the dynamics describing the growth of a cancer of the blood cells characterized by

an abnormal proliferation of leucocytes. In the case of chronic myelogenous leukemia, some models have multiple delays [S24], where stability is affected by both large delays (1 to 8 days) and small delays (1 to 5 minutes) [S25]. Additional examples with delays are encountered in epidemic models due to incubation times [14, 16].

References

[S11] S. Jo and S. G. Massaquoi, "A model of Cerebellum Stabilized and Scheduled Hybrid Long-Loop Control of Upright Balance," *Biological Cybernetics,* vol. 91, pp. 188-202, 2004.

[S12] R. J. Peterka, "Postural Control Model Interpretation of Stabilogram Diffusion Analysis," *Biological Cybernetics,* vol. 82, pp. 335-343, 2000.

[S13] G. Stepan (Ed.), "Delay Effects in Brain Dynamics," *Philosophical Transactions of Royal Society A,* vol. 367, 2009.

[S14] A. Goldbeter, *Biochemical Oscillations and Cellular Rhythms.* Cambridge University Press, Cambridge, 1996.

[S15] B. C. Goodwin, "Oscillatory Behaviour in Enzymatic Control Processes," *Adv. in Enzyme Regulation*, vol. 3, pp. 425-438, 1965.

[S16] I. R. Epstein, "Differential Delay Equations in Chemical Kinetics: Some Simple Linear Model Systems," *Journal of Chemical Physics,* vol. 92, pp. 1702-1712, 1990.

[S17] M. A. Roussel, "The Use of Delay Differential Equations in Chemical Kinetics," *Journal of Physical Chemistry,* vol. 100, pp. 8323-8330, 1996.

[S18] F. H. Feinberg, *Lectures on Chemical Reaction Networks.* University of Wisconsin-Madison, 1979. Available at `http://www.che.eng.ohio-state.edu/~FEINBERG/LecturesOnReactionNetworks/`

[S19] N. MacDonald, "Time Lag in a Model of a Biochemical Reaction Sequence with End-Product Inhibition," *Journal of Theoretical Biology*, vol. 67, pp. 549-556, 1977.

[S20] E. D. Sontag, "Asymptotic Amplitudes and Cauchy Gains: A Small-Gain Principle and an Application to Inhibitory Biological Feedback," *Systems and Control Letters,* vol. 47, pp. 167-179, 2002.

[S21] T. olde Scheper, D. Klinkenberg, C. Pennartz, and J. van Pelt, "A Mathematical Model for the Intracellular Circadian Rhythm Generator," *Journal of Neuroscience,* vol. 19, pp. 40-47, 1999.

[S22] S. Bernard, B. Čajavec, L. Pujo-Menjouet, M. C. Mackey, and H. Herzel, "Modelling Transcriptional Feedback Loops: The Role of Gro/TLE1 in Hes1 Oscillations," *Philosophical Transactions of Royal Society A,* vol. 364, pp. 1155-1170, 2006.

[S23] J. M. Mahaffy, J. Bélair, and M. Mackey, "Hematopoietic Model with Moving Boundary Condition and State Dependent Delay: Applications in Erythopoiesis," *Journal of Theoretical Biology,* vol. 190, pp. 135-146, 1998.

[S24] R. DeConde, P. S. Kim, D. Levy, and P. P. Lee, "Post-Transplantation Dynamics of the Immune Response to Chronic Myelogenous Leukemia," *Journal of Theoretical Biology,* vol. 236, pp. 39-59, 2005.

[S25] S.-I. Niculescu, C.-I. Morărescu, W. Michiels, and K. Gu, "Geometric Ideas in the Stability Analysis of Delay Models in Biosciences," in *Biology and control theory. Current Challenges,* I. Queinnec, S. Tarbouriech, G. Garcia, and S.-I. Niculescu (Eds.), Springer-Verlag, Heidelberg, vol. 357, pp. 230-274, 2007.

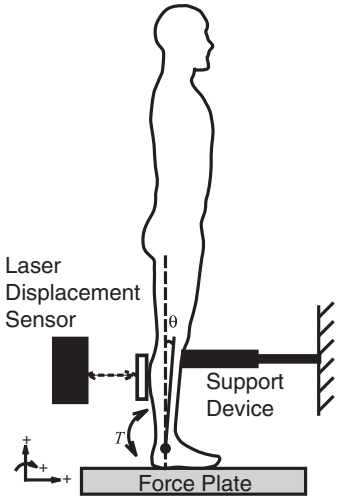

Figure S2: Quiet standing. Analysis of quiet standing offers insight on how humans regulate their vertical posture and puts light on how humans walk without falling. The laser-displacement sensor reads the angular displacement θ of the human body from the vertical, the support device helps support the body at the knees without affecting the natural ankle angle, while the force plate is used to calculate the center of pressure and torques applied by the ankle as the body sways around the vertical. Used with permission of APS. See [19] for full citation information.

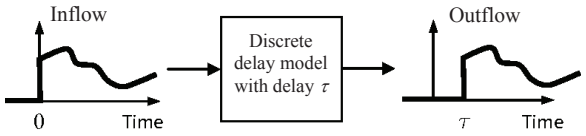

Figure S3: Control diagram for quiet standing. The experimental setup in Figure S2 and its control structure are depicted in this block diagram. An active correction mechanism, which is typically considered as a proportional-derivative controller, emanates from the neural controller and becomes effective after a length of time τ. The neuromusculoskeletal system models the response of the muscles with critically damped second-order dynamics whose natural frequency is ω_n. The human body, which is modeled as an inverted pendulum with inertia I, mass m, and center of mass at height h, responds to the torques originating from the neuromusculoskeletal system and the mechanical controller representing the mechanics of muscles. The electromyography signals shown here are measured at the ankles. Used with permission of APS. See [19] for full citation information.

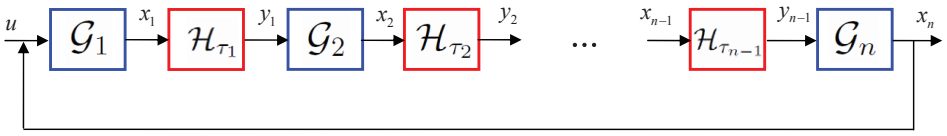

Figure S4: Block diagram of enzyme-activation mechanisms. A cascade of systems is used in [S20] to model the enzyme-activation mechanisms with delays. In this model, the production rate of the enzyme E_i depends on the production rate of the enzyme E_{i-1}. The effect of E_{i-1}, however, takes place after a length of time τ_{i-1} elapses. In a biological system, the variable x_i may represent the amount of enzyme E_i available at time t, while $\mathcal{G}_i$ and $\mathcal{H}_{\tau_i}$ represent, respectively, nonlinear dynamics with outputs x_i and y_i. Moreover, the action u on $\mathcal{G}_1$ can be inhibited by the final product x_n. The stability, oscillation characteristics, and chaos of the closed-loop system are of interest.

10 Sidebar 4: Delays in Operations Research

The main components of a supply chain model are the inventories, the communication medium, the decision-making dynamics associated with a human in the loop, the production and supplies, and the transportation medium. Among these components, the transportation, decision-making, and production are primary sources of delay as shown in Figure S5 [6,7,S26,S27]. One of the objectives in a supply chain system is to maintain a constant inventory as a safety stock, while responding to dynamically changing customer demand, and receiving additional supplies that are not instantaneously available due to transportation delays. Delays can cause either excessive or insufficient inventories, when a manager is unable to replenish the inventories in a timely manner.

Consider the stock-acquisition model

$$\frac{d}{dt}O(t) = -\alpha_{SL}O(t) - (\alpha_S - \alpha_{SL})O(t-h) + r(t), \tag{S9}$$

$$r(t) = \frac{1}{T}(\alpha_{SL}\hat{\tau} + 1 + \alpha_S T)L(t) - \frac{1}{T}(\alpha_{SL}\hat{\tau} + 1)L(t-T), \tag{S10}$$

where $O(t)$ is the manager's ordering dynamics, the positive constants α_{SL} and α_S are proportional controller gains regulating discrepancies in the supply line and in the inventory, respectively, $h > 0$ is the manufacturing lead-time delay, $r(t)$ is the nonhomogeneous part of (S9), and $\hat{\tau}$ is an estimate of h [S27]. The customer demand forecaster $L(t)$ tracks the customer demand, and smoothes the demand over a period T.

The model (S9)-(S10), which is supported by experiments [S27], contains the key components of a supply chain as shown in Figure S6. Equations (S9)-(S10) can also express the inventory variations $N(t)$ influenced by the demand $D(t)$ and products ordered at $t-\tau$, that is, $dN(t)/dt = O(t-\tau) - D(t)$. We can then determine controller gains such that $N(t)$ behaves in a desirable way, and calculate the delay values that do not destabilize $N(t)$ for a given controller.

The characteristic equation of the dynamics in (S9) is given by

$$f(s;h) = s + \alpha_{SL} + (\alpha_S - \alpha_{SL})e^{-\tau s} = 0, \tag{S11}$$

where τ is the manufacturing lead-time delay. Multiple delays can be considered to account for the decision-making delay h_1, the manufacturing lead time h_2, and the transportation time h_3 [S28]. In this case, the governing dynamics in (S9) can be reformulated, leading to the three-delay characteristic

equation

$$f(s; h_1, h_2, h_3) = s + \alpha_{SL}(e^{-h_1 s} - e^{-(h_1+h_2)s}) + \alpha_S e^{-(h_1+h_2+h_3)s} = 0. \quad \text{(S12)}$$

The characteristic equations (S11) and (S12) can be combined with the stability analysis technique presented in the section "Multiple-Delay Case" in order to investigate the stability with respect to either the delays or system parameters. Note that the models (S11) and (S12) represent the characteristic equations of the ordering dynamics $O(t)$ of the managers. The ordering dynamics can be combined with $\tilde{N}(s) = \frac{1}{s}\left(\tilde{O}(s)e^{-\overline{\tau}s} - \tilde{D}(s)\right)$ to study the stability of the inventory dynamics $N(t)$, where $\overline{\tau}$ is the total amount of delay between ordering new products and the arrival of these products in the inventories, and $\tilde{O}(s)$, $\tilde{D}(s)$, and $\tilde{N}(s)$ are the Laplace transforms of ordering, customer demand, and inventory levels, respectively.

References

[S26] D. Helbing, S. Lämmer, T Seidel, P. Šeba, and T. Płatkowski, "Physics, Stability and Dynamics of Supply Networks," *Physical Review E*, vol. 70, article no. 066116, 2004.

[S27] J. D. Sterman, "Modeling Managerial Behavior: Misperceptions of Feedback in a Dynamics Decision Making Experiment," *Management Science*, vol. 35, pp. 321-339, 1989.

[S28] R. Sipahi and I. I. Delice, "Stability of Inventory Dynamics in Supply Chains with Three Delays," *International Journal of Production Economics,* vol. 123, pp. 107-117, 2010.

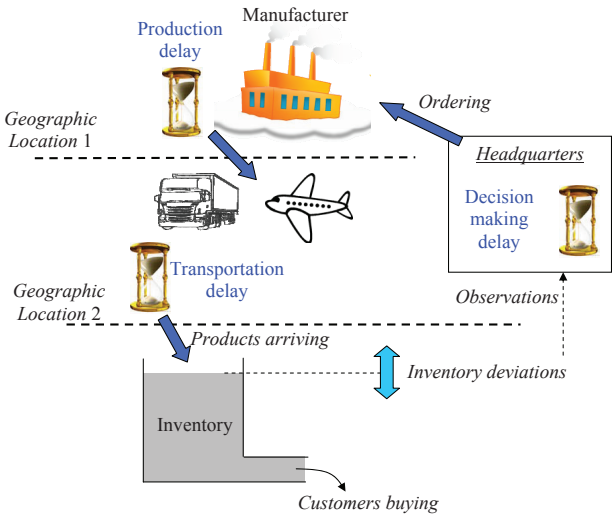

Figure S5: Supply chains and delays. Supply-chain systems are examples of interconnected supply-demand points that share products and information in order to regulate inventories and optimally respond to customer demands. Various sources of delay in supply chains include decision-making delays, transportation lines, and lead times in manufacturing facilities. Delays in supply chains influence every stage of the supply-demand chain, causing financial losses, inefficiencies, and reduced quality-of-service.

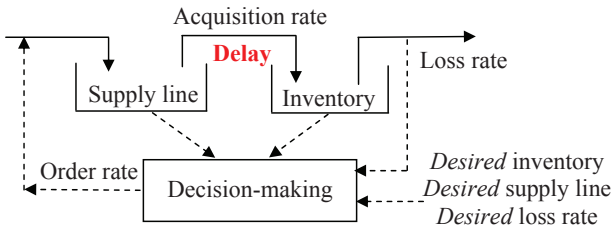

Figure S6: Inventory acquisition model [S27]. This model represents the flow of products in a supply chain, where decision-making adjusts the orders needed to respond to each customer's buying rate, that is, the loss rate. Due to the presence of delays, the orders placed earlier by the decision maker traverse the supply line first and then arrive at the inventory after a delay.

11 Sidebar 5: Stabilizing Predictors

Delay terms may also arise when designing state predictors and observers. To explain the main ideas, we consider the linear system

$$\dot{x}(t) = Ax(t), \tag{S13}$$

$$y(t) = Cx(t). \tag{S14}$$

Since (S13)-(S14) is time invariant, a prediction $y_p(t)$ of the output $y(t)$ over a time-delay interval of length τ can be generated from a model of the system given by

$$\dot{z}(t) = Az(t),$$

$$y_p(t) = Cz(t).$$

The observer design includes a control term in the predictor that depends on the difference $y_p(t-\tau) - y(t)$ between the outputs. We then obtain the predictor

$$\dot{z}(t) = Az(t) + K(y_p(t-\tau) - y(t)), \tag{S15}$$

$$y_p(t) = Cz(t), \tag{S16}$$

which can be combined with (S13)-(S14) to express the error dynamics as

$$\dot{e}(t) = Ae(t) + KCe(t-\tau), \tag{S17}$$

where $e(t) = z(t-\tau) - x(t)$ is the error, and the gain K is selected to guarantee the stability of the error dynamics, for instance, by following the stability analysis techniques explained in the section "Delay Differential Equations and the Characteristic Equation".

For control systems with delays, the detrimental effects of delays are minimized by including predictors in the control feedback loop. The controller then uses either the prediction of the plant state variable or output for feedback, instead of the plant state variable and outputs. This type of delay compensation is the basis for the Smith predictor [32, S29], as well as schemes based on finite spectrum assignment [S30]. Prediction-based schemes are applicable to unstable open-loop systems only if stabilization of the predictor is addressed.

References

[S29] Z. J. Palmor, "Time-Delay Compensation - Smith Predictor and its Modifications," pp. 224-237, in S. Levine (ed.) *The Control Handbook*, CRC and IEEE Press, New York, 1996.

[S30] A. Manitius and A. Olbrot, "Finite Spectrum Assignment Problem for Systems with Delays," *IEEE Transactions on Automatic Control*, vol. 24, pp. 541-552, 1979.

12 Sidebar 6: Stabilizing Unstable Periodic Orbits in Chaotic Systems

Delays can be used to stabilize unstable periodic orbits that appear in chaotic systems. Questions of observability and reconstructibility in both linear and nonlinear dynamical systems concern the availability of sufficient information in the output space that can be used to reconstruct the behavior of the system in state space. The following definitions are used to state the main results in delay embedding, time-series prediction, and stabilizing chaotic systems.

Definition 2 *The topological spaces X and Y are topologically equivalent if a continuous mapping $f : X \to Y$ exists with a continuous inverse f^{-1}.*

Definition 3 *If $f : X \to Y$, where X and Y are topological spaces, is a continuous mapping with a continuous inverse $f^{-1} : f(X) \to X$ from its range $f(X) \subset Y$ to its domain X, then the function f is an* embedding.

Consider the input-free dynamical system

$$\dot{x}(t) = f(x(t)), \tag{S18}$$

$$y(t) = h(x(t)), \tag{S19}$$

where $x \in M$, M is an n-dimensional manifold, and the output y is a scalar. Given only the output measurements, we are interested in determining information about the phase-space of system (S18)-(S19), in particular, the geometric behavior of the state x. We assume that x is bounded, and eventually resides on an attractor A.

Definition 4 *Let ϕ be a flow on M, let $\tau > 0$, and let $h : M \to \mathbb{R}$ be a smooth measurement function. The delay coordinate map with embedding delay τ, $F(h, \phi, \tau) : M \to \mathbb{R}^m$, is defined by $x \mapsto F(h, \phi, \tau) = \left(h(x), h(\phi^{-\tau}(x.....h(\phi^{-2\tau}(x)), \ldots, h(\phi^{-(m-1)\tau}(x))\right)$.*

Definition 5 *The subset $U \subset X$ of a topological space is* residual *if it contains the intersection of a countable number of open dense subsets. A property is called generic if it holds on a residual set.*

Baire's theorem guarantees that a residual set is not empty, but may have arbitrarily small measure [S31]. Furthermore, we know that every d-dimensional manifold can be embedded into $\mathbb{R}^{2d+1}$ [S32]. Takens' embedding theorem provides a particular embedding using delay mappings to reconstruct the state space of the original dynamical system [S33].

Theorem 6 *(Takens [S33]) Let M be a compact manifold of dimension d, and let $\tau > 0$ be the embedding delay. For the nonlinear system (f, h, τ), if f is a smooth vector field on M with flow ϕ and $h : M \to \mathbb{R}$ is a smooth measurement function, then the delay coordinate map $F(h, \phi, \tau) : M \to \mathbb{R}^{2d+1}$ is an embedding.*

The output function $y(t) = h(x(t))$ is usually dictated by the available sensors, and may not be mathematically available. The measurement function $h(\cdot)$ is piecewise constant, and the assumptions and conclusions of Theorem 6 are not achieved in practice. Nevertheless, delay-embedding approaches are used in order to predict the future outputs of nonlinear systems [S34] and control chaotic systems [S35–S37]. The prediction of future outputs is achieved as follows. Using the collection of delay mappings $F(t), F(t+1), \ldots, F(t+\ell)$, a model of a dynamical system whose state is $F(t)$ can be obtained by either a linear or nonlinear identification algorithm. For example, we can obtain the matrix G such that $F(t+1) = GF(t)$ [S34]. The delay-embedding and prediction algorithm are illustrated in Figure S7.

Chaotic systems, which are sensitive to initial conditions, can also be characterized by attractor sets containing infinitely many unstable periodic orbits. These properties can be exploited to design delayed feedback for physical chaotic systems [86]. The discussion below is based on the OGY methods [S38] used to suppress chaos in dynamical systems by driving the trajectories to a limit cycle [S39].

Consider the dynamical system

$$\dot{x}(t) = f(x(t), u(t), t), \tag{S20}$$

$$y(t) = h(x(t)), \tag{S21}$$

where $x(\cdot) \in \mathbb{R}^n$, and u and y are scalars. Assume that, for $u(t) = 0$, the system has an unstable periodic orbit $x_0(t)$ of period T that satisfies $\dot{x}_0 = f(x_0, 0, t)$ and $x_0(t+T) = x_0(t)$ among its potentially infinitely many periodic orbits. Let $y_0(t) = h(x_0(t))$, and let the feedback input with multiple delays be given by

$$u(t) = K \left[(1-R) \sum_{n=1}^{\infty} R^{n-1} y(t - nT) - y(t) \right],$$

where $|R| < 1$. To analyze the stability of the closed-loop system, we use a perturbation approach by considering the small state perturbations $\delta x = x_0(t) - x(t)$. Note that for chaotic systems, the trajectory $x(t)$ becomes

infinitesimally close to an unstable periodic orbit due to the presence of infinitely many unstable periodic orbits, and since the attractor has a finite dimension. The linearized closed-loop system is given by

$$\delta\dot{x} = A(t)\delta x(t) + KB(t)\left[(1-R)\sum_{n=1}^{\infty} R^{n-1}\delta x(t-nT) - \delta x(t)\right],$$

where $A(t)$ and $B(t)$ are periodic matrices. Noting that

$$\delta x(t-nT) = e^{-n\Lambda T}\delta x(t),$$

where $\Lambda \in \mathbb{R}$ is the Floquet exponent [S38], the stabilization problem is reduced to that of studying the stability of the closed-loop system

$$\delta\dot{x} = [A(t)\delta x(t) + KH(\Lambda)B(t)]\delta x(t),$$

where

$$H(\Lambda) = (1-e^{-\Lambda T})/(1-Re^{-\Lambda T}).$$

Finding Λ typically requires the solution of a transcendental equation, and for some special orbits, Λ can be obtained [S38]. Finally, this approach can be experimentally implemented to stabilize various physical systems [S40, S41].

Example 9 *This example illustrates the time-delay embedding application of Theorem 6. Consider the Lorenz oscillator described by the equations*

$$\begin{aligned}
\frac{dx_1}{dt} &= a(x_2 - x_1),\\
\frac{dx_2}{dt} &= x_1(b - x_3) - x_2,\\
\frac{dx_3}{dt} &= x_1x_2 - cx_3,
\end{aligned}$$

where a, b, and c are real constants. For the particular choice $a = 10$, $b = 28$, and $c = 8/3$, we obtain the attractor shown in Figure S8. By measuring $y = h(x) = x_1$ and using a delay of $\tau = 1$ s, the reconstructed attractor is shown in Figure S9. While the reconstructed attractor with this projection approach looks different from the actual attractor, the attractor can be used to predict the trajectory of x_1, x_2, and x_3. ■

References

[S31] R.-L. Baire, "Sur les fonctions de variables réelles," *Annali di Matematica Pura ed Applicata,* Series 3, vol. 3, pp. 1-123, 1899.

[S32] M. Adachi, *Embedding and Immersions.* American Mathematical Society, Providence, RI, 1962.

[S33] F. Takens, "Detecting strange attractors in turbulence," in D. A. Rand and L.-S. Young, *Dynamical Systems and Turbulence.* Springer-Verlag, vol. 898, pp. 366-381, 1981.

[S34] M. Casdagli, S. Eubank, J. D. Farmer, and J. Gibson, "State Space Reconstruction in the Presence of Noise," *Physica D,* vol. 51, pp. 52-98, 1991.

[S35] E. Ott, C. Grebogi, and J. A. Yorke, "Controlling Chaos," *Physical Review Letters,* vol. 64, article no. 1196, 1990.

[S36] P. So and E. Ott, 'Controlling Chaos Using Time Delay Coordinates via Stabilization of Periodic Orbits," *Physical Review E,* vol. 51, pp. 2955-2962, 1995.

[S37] X. Yu, G. Chen, Y. Xia, Y. Song, and Z. Cao, "An Invariant-Manifold-Based Method for Chaos Control," *IEEE Trans on Circuits & Systems-I: Fundamental Theory and Applications,* vol. 48, pp. 930-937, 2001.

[S38] K. Pyragas, "Delayed Feedback Control of Chaos," *Philosophical Transactions of Royal Society A,* vol. 364, pp. 2309-2334, 2006.

[S39] E. Ott, *Chaos in Dynamical Systems.* Cambridge University Press, Cambridge, 1993.

[S40] T. Shinbrot, W. Ditto, C. Grebogi, E. Ott, M. L. Spano, and J. A. Yorke, "Using the Sensitive Dependence of Chaos to Direct Orbits to Targets in an Experimental Chaotic Systems," *Physical Review Letters,* vol. 68, article no. 2863, 1992.

[S41] A. Jnifene, "Active Vibration Control of Flexible Structures Using Delayed Position Feedback," *Systems & Control Letters*, vol. 56, pp. 215-222, 2007.

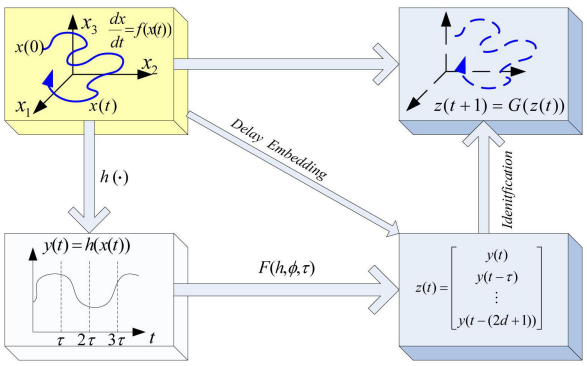

Figure S7: The embedding and prediction algorithms. The mapping $F(h, \phi, \tau)$ provides delay embedding to reconstruct the vector $z(t)$, which can then be used to identify the mapping G and predict $z(t+1)$. Note that the first entry of $z(t)$ is the output $y(t)$.

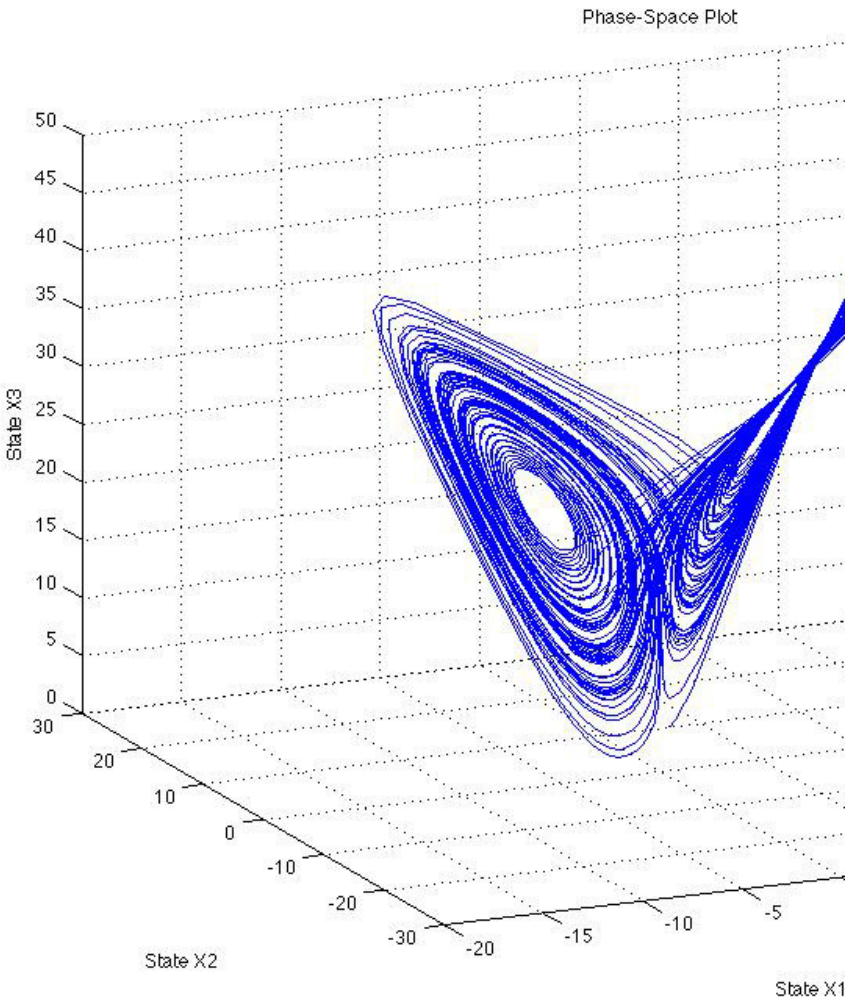

Figure S8: The Lorentz attractor. This attractor, which is in $\mathbb{R}^3$, is composed of an infinite number of unstable limit cycles. For the particular choice of the parameters in Example 9, all trajectories converge to the chaotic attractor. This attractor illustrates both the long-term unpredictability and the boundedness of the trajectories.

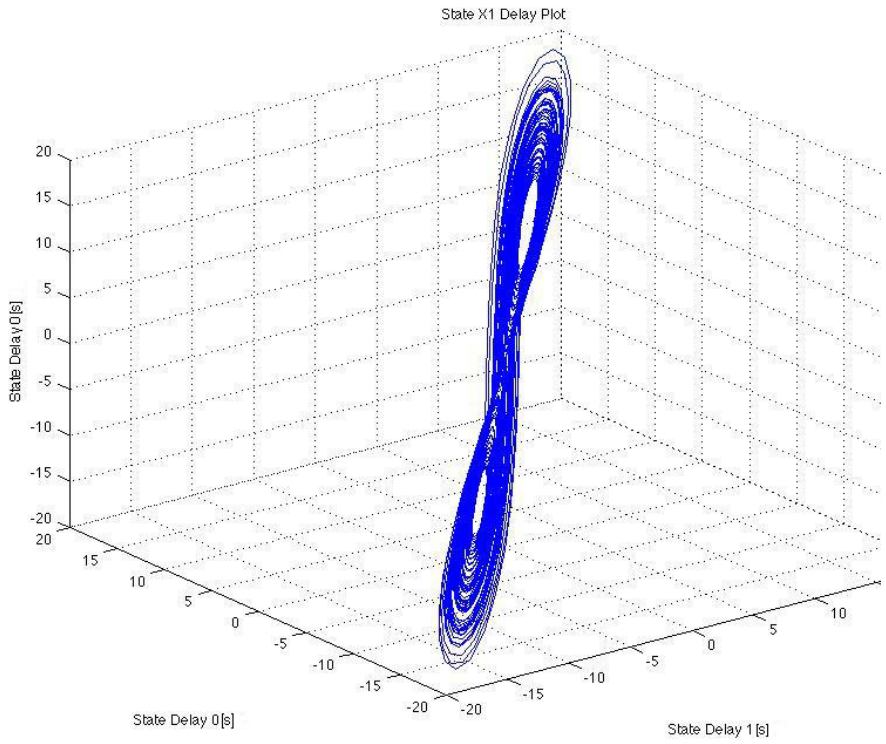

Figure S9: The reconstructed Lorentz attractor. The reconstruction is based on the output measurement $y = x_1$, which is projected onto $\mathbb{R}^3$ for the embedding dimension $n = 2d + 1 = 7$. While the reconstructed shape is not identical to the attractor in Figure S8, the first three components of $F(t)$ shown in the reconstructed attractor comprise the signals $y(t)$, $y(t-1)$, and $y(t-2)$. Theorem 6 is used to guarantee that the reconstructed attractor using a sufficient number of delays is the image of an embedding mapping of the original attractor. The delayed signals can be used to either stabilize the Lorenz system or obtain a predictive model of the output $y(t)$.

13 Sidebar 7: Numerical Stability and Bifurcation Analysis

The MATLAB package DDE-BIFTOOL provides numerical bifurcation and stability analysis of delay differential equations with several fixed constant or state-dependent delays [80]. This package contains routines for the computation, continuation, and stability analysis of steady-state solutions, their Hopf and fold bifurcations, periodic solutions, and connecting orbits. A stability analysis of steady-state solutions is achieved through computing approximations and corrections of the rightmost characteristic roots using a linear multistep method. Periodic solutions, their Floquet multipliers, and connecting orbits are computed using piecewise polynomial collocation on adaptively refined meshes. An overview of DDE-BIFTOOL for stabilization problems is presented in [S42]. Additional numerical methods that can compute the rightmost roots of LTI DDEs include the quasi-polynomial mapping-based rootfinder (QPmR) technique [S43] and pseudospectral differencing methods [S44].

References

[S42] D. Roose, T. Luzyanina, K. Engelborghs, and W. Michiels. "Software for stability and bifurcation analysis of delay differential equations and application to stabilization," In *Advances in Time-Delay Systems.* Springer-Verlag, pp. 167-182, 2004.

[S43] T. Vyhlídal, and P. Zítek, "Quasipolynomial mapping based rootfinder for analysis of time delay systems," *IFAC Workshop on Time Delay Systems*, Rocquencourt, France, 2003. Available at `http://www.ifac-papersonline.net/`.

[S44] D. Breda, S. Maset, and R. Vermiglio, "Pseudospectral Differencing Methods for Characteristic Roots of Delay Differential Equations", *SIAM Journal of Scientific Computing,* vol. 27, pp. 482-495, 2006.